Cell Biology
Cancer Biology

Plectin-mediated cytoskeletal crosstalk as a target for inhibition of hepatocellular carcinoma growth and metastasis

Reviewed Preprint
v2 • January 27, 2025
Revised by authors

Reviewed Preprint
v1 • October 16, 2024

Zuzana Outla, Gizem Oyman-Eyrilmez, Katerina Korelova, Magdalena Prechova, Lukas Frick, Lenka Sarnova, Piyush Bisht, Petra Novotna, Jan Kosla, Patricia Bortel, Yasmin Borutzki, Andrea Bileck, Christopher Gerner, Mohammad Rahbari, Nuh Rahbari, Emrullah Birgin, Bibiana Kvasnicova, Andrea Galisova, Katerina Sulkova, Andreas Bauer, Njainday Jobe, Ondrej Tolde, Eva Sticova, Daniel Rosel, Tracy O'Connor, Martin Otahal, Daniel Jirak, Mathias Heikenwälder, Gerhard Wiche, Samuel M Meier-Menches, Martin Gregor

Laboratory of Integrative Biology, Institute of Molecular Genetics of the Czech Academy of Sciences, Prague, Czech Republic • Institute of Molecular Cancer Research, University of Zurich, Zurich, Switzerland • Division of Chronic Inflammation and Cancer, German Cancer Research Center, Heidelberg, Germany • Department of Analytical Chemistry, University of Vienna, Vienna, Austria • Institute of Inorganic Chemistry, University of Vienna, Vienna, Austria • Joint Metabolome Facility, Medical University of Vienna and University of Vienna, Vienna, Austria • Department of Surgery, University Hospital Mannheim, Medical Faculty Mannheim, University of Heidelberg, Mannheim, Germany • Department of General and Visceral Surgery, Ulm University Hospital, Ulm, Germany • Department of Natural Sciences, Faculty of Biomedical Engineering, Czech Technical University in Prague, Kladno, Czech Republic • Department of Radiodiagnostic and Interventional Radiology, Institute for Clinical and Experimental Medicine, Prague, Czech Republic • Department of Physics, University of Erlangen-Nuremberg, Erlangen, Germany • Department of Cell Biology, Faculty of Science, Charles University, BIOCEV, Vestec, Czech Republic • Department of Clinical and Transplant Pathology, Institute for Clinical and Experimental Medicine, Prague, Czech Republic • Department of Pathology, Third Faculty of Medicine, Charles University, Prague, Czech Republic • Department of Biology, North Park University, Chicago, United States • Department of Biochemistry and Cell Biology, Max F. Perutz Laboratories, University of Vienna, Vienna, Austria

eLife Assessment

This **valuable** study investigated the role of PLECTIN, a cytoskeletal crosslinker protein, in hepatocellular carcinoma development and progression. Using a liver-specific Plectin knockout mouse model, the authors showed **solid** evidence that PLECTIN is critical for hepatocarcinogenesis, since inhibition of PLECTIN suppressed tumor formation in multiple models. They also show that PLECTIN is key for HCC invasion and metastasis. They show a correlation between PLECTIN inhibition and attenuated FAK, MAPK/ERK, and PI3K/AKT signaling.

https://doi.org/10.7554/eLife.102205.2.sa4

Abstract

The most common primary malignancy of the liver, hepatocellular carcinoma (HCC), is a heterogeneous tumor entity with high metastatic potential and complex pathophysiology. Increasing evidence suggests that tissue mechanics plays a critical role in tumor onset and progression. Here we show that plectin, a major cytoskeletal crosslinker protein, plays a crucial role in mechanical homeostasis and mechanosensitive oncogenic signaling that drives hepatocarcinogenesis. Our expression analyses revealed elevated plectin levels in liver tumors, which correlated with poor prognosis for HCC patients. Using autochthonous and orthotopic mouse models we demonstrated that genetic and pharmacological inactivation of plectin potently suppressed the initiation and growth of HCC. Moreover, plectin targeting potently inhibited the invasion potential of human HCC cells and reduced their metastatic outgrowth in the lung. Proteomic and phosphoproteomic profiling linked plectin-dependent disruption of cytoskeletal networks to attenuation of oncogenic FAK, MAPK/Erk, and PI3K/AKT signatures. Importantly, by combining cell line-based and murine HCC models, we show that plectin inhibitor plecstatin-1 (PST) is well-tolerated and potently inhibits HCC progression. In conclusion, our study demonstrates that plectin-controlled cytoarchitecture is a key determinant of HCC development and suggests that pharmacologically induced disruption of mechanical homeostasis may represent a new therapeutic strategy for HCC treatment.

Introduction

Mounting evidence indicates that tissue mechanics plays a pivotal role in cancer cell and stromal cell behavior. Tumor progression is typically associated with a pathological increase of tissue stiffness caused by excessive deposition, crosslinking, and aberrant organization of dense extracellular matrix (ECM) fibers. Increasing tissue rigidity drives tumor invasion and malignancy and correlates with poor patient survival[1,2].

At the cellular level, both tumor and stromal cells respond to altered mechanical properties of the extracellular milieu by translating physical cues into mechanosensitive signaling pathways. This conversion relies on focal adhesions (FAs), clusters of integrin receptors facilitating the link between the ECM and the cytoskeleton. Integrin-mediated adhesion induces the activation of FAK, MAPK/Erk, and PI3K/AKT pathways, leading to increased cell survival, migration, and invasion[3–5]. Subsequent activation of Rho-dependent pathways results in higher cytoskeletal tension and force transmission across FAs, thus establishing a mechanical reciprocity between ECM viscoelasticity and actomyosin- generated cytoskeletal tension. Importantly, many genes encoding components of the ECM- cytoskeletal axis and their regulators (e.g. *αSMA*, *ITGβ*, *LMNA*, *ROCK*, and *COL*) are controlled by tension-dependent transcription[6,7]. This creates a difficult-to-break positive feedback loop leading to cellular and matrix stiffening, further promoting the aggressive, pro-proliferative, and invasive tumor cell phenotype.

Emerging therapeutic strategies aimed at tumor mechanics and mechanotransduction include the targeting of the ECM and ECM modulators (e.g. lysyl oxidase and angiotensin), depletion of stromal myofibroblasts, and integrin receptors[2,3]. Other approaches target cytoskeleton-mediated downstream cellular response to tissue stiffening (e.g. Rho-dependent actomyosin-generated contractile forces[8]). We hypothesized that another efficacious strategy could be inactivation of cytoskeletal crosslinker proteins (so-called cytolinkers)[9,10], large proteins of the plakin protein family, responsible for maintaining cellular architecture. The best-studied example, a prototypical cytolinker plectin is a well-established regulator of cellular tensional homeostasis and

mechanotransduction[10] which is upregulated in various tumors[11,12]. Through its canonical actin-binding domain (ABD[13]) and intermediate filament (IF)-binding domain (IFBD[14]), plectin crosslinks actin with IF networks and recruits them to cell adhesions, including FAs. Plectin deletion or mutation results in cytoskeletal reconfiguration accompanied by altered mechanical properties, such as cellular stiffness, stress propagation, and traction force generation[15–18]. In addition, plectin-dependent changes in cell adhesions[18–21] and cytoskeletal tension[17,18,20–22] are associated with aberrant integrin-mediated mechanosignaling[20,21]. Although multiple reports have linked plectin with tumor malignancy[12] and other pathologies[10,23], mechanistic insights into how plectin functionally contributes to carcinogenesis remain largely unknown.

A malignancy with a well-known link to overproduction of ECM components is hepatocellular carcinoma (HCC), the most common type of liver cancer. Repeated rounds of hepatocyte damage and renewal due to a number of etiologies, most commonly chronic viral infection, alcohol abuse, or a diet rich in fats and sugars, creates a pro-inflammatory environment in the liver. Activated hepatic stellate cells adopt a myofibroblast phenotype and increase production and deposition of ECM components leading to liver fibrosis which can eventually progress to liver cirrhosis. Up to 90% of HCC cases occur on a background of liver fibrosis or cirrhosis, suggesting a causal link between increased deposition of ECM components and liver carcinogenesis. Consistent with this idea, plectin mRNA has been found to be upregulated in liver carcinomas, especially in later stages of disease[11]. Thus, changes in the interactions between the cytoskeleton and ECM may be important in HCC progression, particularly during the transition from local to metastatic malignancy.

Here we explore the role of plectin in the development and dissemination of HCC. Using publicly available HCC sequencing data and biopsies from HCC patients we identify plectin as a novel HCC marker associated with a malignant phenotype and poor survival. To explore the role of plectin in hepatocarcinogenesis, we use a genetic mouse model with liver-specific plectin ablation ($Ple^{\Delta Alb}$). In this model, plectin deficiency suppresses tumor initiation and growth. We further demonstrate that CRISPR/Cas9-engineered human HCC cell lines with inactivated plectin display limited migration, invasion, and anchorage-independent proliferation which correlates with their reduced metastatic outgrowth in the lung. By comprehensive proteomic analysis, we show that plectin inactivation attenuates oncogenic FAK, MAPK/Erk, and PI3K/AKT signaling signatures. Finally, our work identifies the ruthenium-based plecstatin-1 (PST), as a candidate drug that can mimic the genetic ablation of plectin, thus providing a robust pre-clinical proof-of-concept for PST in the treatment of HCC. Our study implicates plectin as a potent driver of HCC, highlights its importance in metastatic spread, and points to potential novel treatment options.

Results

Plectin levels are elevated in HCC and predict a poor prognosis

Using 17 distinct HCC patient datasets, we confirmed that *plectin* expression is consistently and significantly increased in HCC samples when compared to non-tumor (NT) liver tissues (**Fig. 1A**). The analysis of data from The Cancer Genome Atlas (TCGA) confirmed elevated *plectin* expression in HCC, irrespective of HCC etiology or gender (**Figure 1**—figure supplement 1A-D). To assess whether high plectin expression is typical for a specific subpopulation of HCC patients, we created t-SNE plots and compared plectin expression patterns with those of molecular subclasses of Dr. Changś and Dr. Boyault's classification[24,25]. Although we observed local clusters of patients with higher or lower plectin expression levels, they did not seem to be associated with any of the largest clusters or subgroups (**Figure 1**—figure supplement 1E). Strikingly, using higher tertile

expression as the cut-off, higher *plectin* mRNA levels were associated with a significant decrease in recurrence-free survival (**Fig. 1B**). A similar trend was observed across 8 distinct HCC datasets (**Figure 1**—figure supplement 1F).

Consistent with expression analysis, quantitative immunofluorescence microscopy of 19 human HCC tissue sections revealed a significant increase of plectin fluorescence intensities in tumor (T) compared to adjacent non-tumor (NT) tissue, with plectin perimembraneous enrichment in tumor hepatocytes (**Fig. 1C**; **Figure 1**—figure supplement 1G). Next, we compared plectin expression levels by immunoblotting in a panel of human HCC cell lines, which represent distinct stages of HCC development[24]. Consistent with mRNA and immunofluorescence analyses, poorly differentiated mesenchymal-like HCC cell lines (characterized by low E-cadherin and high vimentin levels) displayed elevated plectin levels, coinciding with higher migration speed when compared to well-differentiated HCC cell lines (**Fig. 1D,E**).

To validate our findings in a well-established chemical carcinogen murine HCC model, we analyzed plectin expression in hepatic tumors formed 46 weeks after diethylnitrosamine (DEN) injection in C57BI/6J mice (**Fig. 1F**). Both quantitative immunofluorescence and immunoblot analyses indicated elevated plectin levels in T versus NT liver tissue (**Fig. 1C,G**,H; **Figure 1**—figure supplement 1H). Moreover, enhanced plectin signal along hepatocyte membranes closely resembled the staining pattern found in patient HCC sections (**Fig. 1C**), suggesting reliable translation from the human setting. Together, these results show that elevated plectin is associated with HCC progression both in human patients and animal model and indicates robust prognostic potential for patient survival.

Plectin promotes hepatocarcinogenesis

To determine the functional consequences of plectin loss in liver tumor development, we analyzed the formation of DEN-induced HCCs in mice lacking plectin expression in the liver using magnetic resonance imaging (MRI). To achieve liver-specific plectin deletion, mice carrying a floxed plectin sequence ($Ple^{fl/fl}$) were crossed to mice expressing the Cre recombinase under the liver-specific albumin promoter (*Alb-Cre*). The resulting mice ($Ple^{\Delta Alb}$) lack plectin expression in the liver[26]. Remarkably, MRI screening 32 and 44 weeks post-injection revealed a significant reduction of tumor number and volume in $Ple^{\Delta Alb}$ mice compared to $Ple^{fl/fl}$ controls (**Fig. 2A-C**). Decreased tumor burden in the second cohort of $Ple^{\Delta Alb}$ mice was confirmed macroscopically 44 weeks after DEN administration (**Fig. 2D,E**). Notably, $Ple^{\Delta Alb}$ mice more frequently formed larger tumors, as reflected by overall tumor size increase (**Fig. 2F**; **Figure 2**—figure supplement 1A), possibly implying reduced migration or increased cohesion of plectin-depleted cells[26,27].

To address plectiń s role in HCC at a cellular level, we genetically manipulated endogenous plectin in well-differentiated Huh7 and poorly differentiated SNU-475 human HCC cell lines[24]. Using the CRISPR/Cas-9 system we generated either knockouts (KO) or cells harboring endogenous plectin with deletion of the IF-binding domain (ΔIFBD) as functional knockouts[18]. (**Figure 2**—figure supplement 1B-D). Gene editing was complemented by treatment with organoruthenium-based compound PST that inactivates plectin function[18,28]. If not stated otherwise, we applied PST in the final concentration of 8 μM, which corresponds to the 25% of IC_{50} for Huh7 cells (**Figure 2**—figure supplement 1E). Consistent with the murine model, plectin inactivation resulted in a reduced number of Huh7 and SNU-475 colonies in a soft agar colony formation assay, with PST treatment closely mimicking the effect of genetic targeting (**Fig. 2G**). Moreover, KO and ΔIFBD SNU-475 colonies were significantly smaller when compared to wild-type (WT) controls, with a similar trend observed for Huh7 cells (**Figure 2**—figure supplement 1F). Collectively, these data demonstrate the inhibitory effect of plectin inactivation on HCC progression in adhesion-independent conditions.

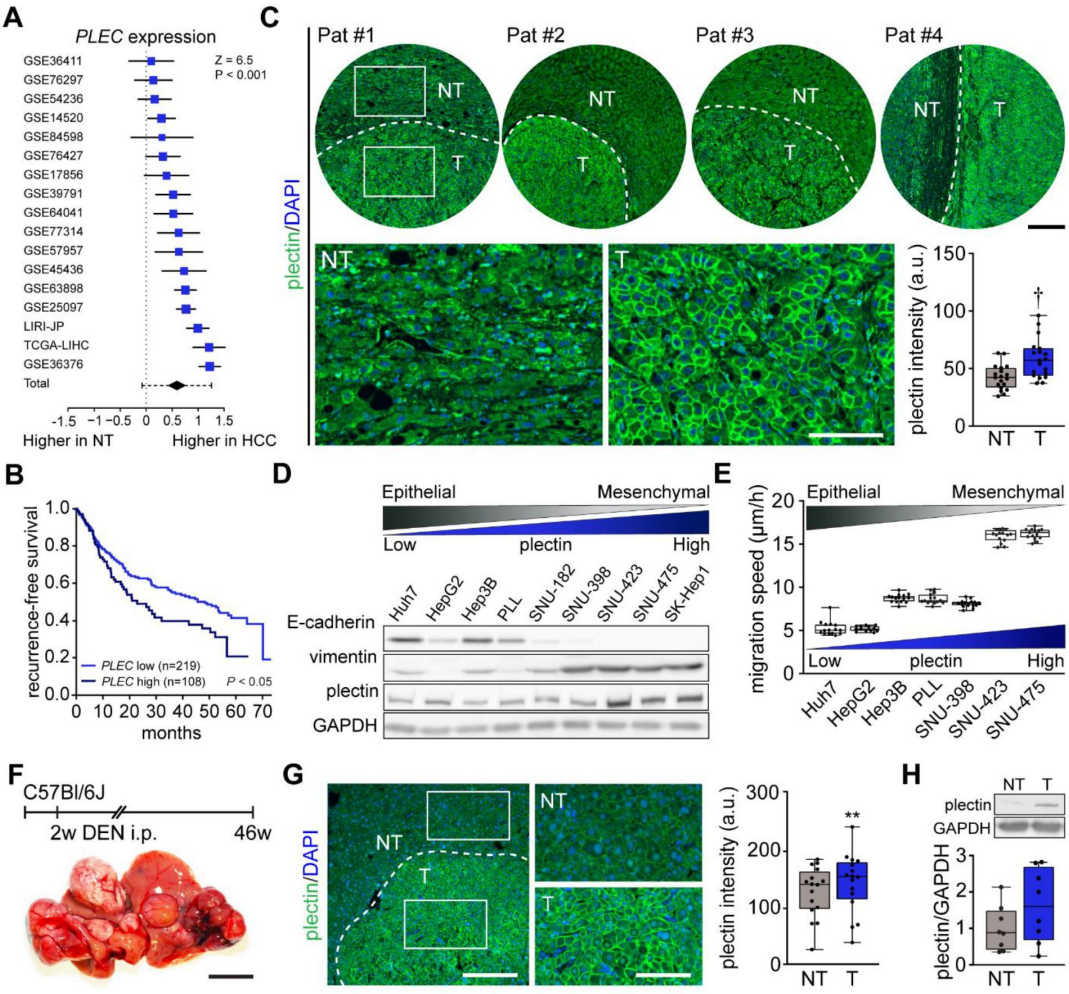

Figure 1.

Plectin elevation in tumor hepatocytes is associated with HCC progression and poor prognosis.

(A) Meta-analysis of differential *plectin* (*PLEC*) mRNA expression in non-tumor (NT) liver and hepatocellular carcinoma (HCC) patients. Blue squares indicate the standardized mean difference (SMD) and 95% confidence interval of individual datasets. The black diamond shows the mean and 95% confidence interval for the combined SMD, while the whiskers indicate the 95% prediction interval. **(B)** Kaplan-Meier curve of recurrence-free survival of HCC patients with low *PLEC* (lower 2 tertiles, $n = 219$) and high *PLEC* (top tertile, $n = 108$) mRNA expression. Log-rank test; $P < 0.05$. **(C)** Representative images of human HCC tissue sections immunolabeled for plectin (green). Nuclei, DAPI (blue). Dashed line, the borderline between non-tumor (NT) and tumor (T) area. Boxed areas, x4 images. Scale bars, 200 and 100 µm (boxed areas). Boxplot shows quantification of plectin fluorescence intensities in NT and T areas. The box represents the median, 25th, and 75th percentile; whiskers reach the last data point; dots, individual patients; $N = 19$. Paired two-tailed *t*-test; $P < 0.001$. (D) Immunoblot analysis of indicated HCC cell lines with antibodies to plectin, E-cadherin, and vimentin. GAPDH, loading control. **(E)** Quantification of the speed of indicated HCC cell lines migrating in the scratch-wound assay. Boxplots show the median, 25th, and 75th percentile with whiskers reaching the last data point; dots, fields of view; $n = 15$ (Huh7), 13 (HepG2), 15 (Hep3B), 15 (PLL), 15 (SNU-398), 15 (SNU-423), 15 (SNU-475) fields of view; $N = 3$. **(F)** Hepatocarcinogenesis was induced in two-week-old C57Bl/6J mice by intraperitoneal injection of DEN. Representative image of the livers with multifocal HCC at 46 weeks post-induction. Scale bar, 1 cm. **(G)** Representative image of DEN- induced HCC section immunolabeled for plectin (green). Nuclei, DAPI (blue). Dashed line, the borderline between non-tumor (NT) and tumor (T) area. Boxed areas, x2 images. Scale bars, 200 and 100 µm (boxed areas). Quantification of plectin fluorescence intensities in NT and T areas. Boxplot shows the median, 25th, and 75th percentile with whiskers reaching the last data point; dots, fields of view; $n = 16$ fields of view; $N = 4$. Paired two-tailed *t*-test; $^{**}P < 0.01$. **(H)** Immunoblot analysis of NT and T liver lysates. The boxplot shows relative plectin band intensities normalized to GAPDH. The box represents the median, 25th, and 75th percentile; whiskers reach the last data point; dots, individual mice; $N = 8$.

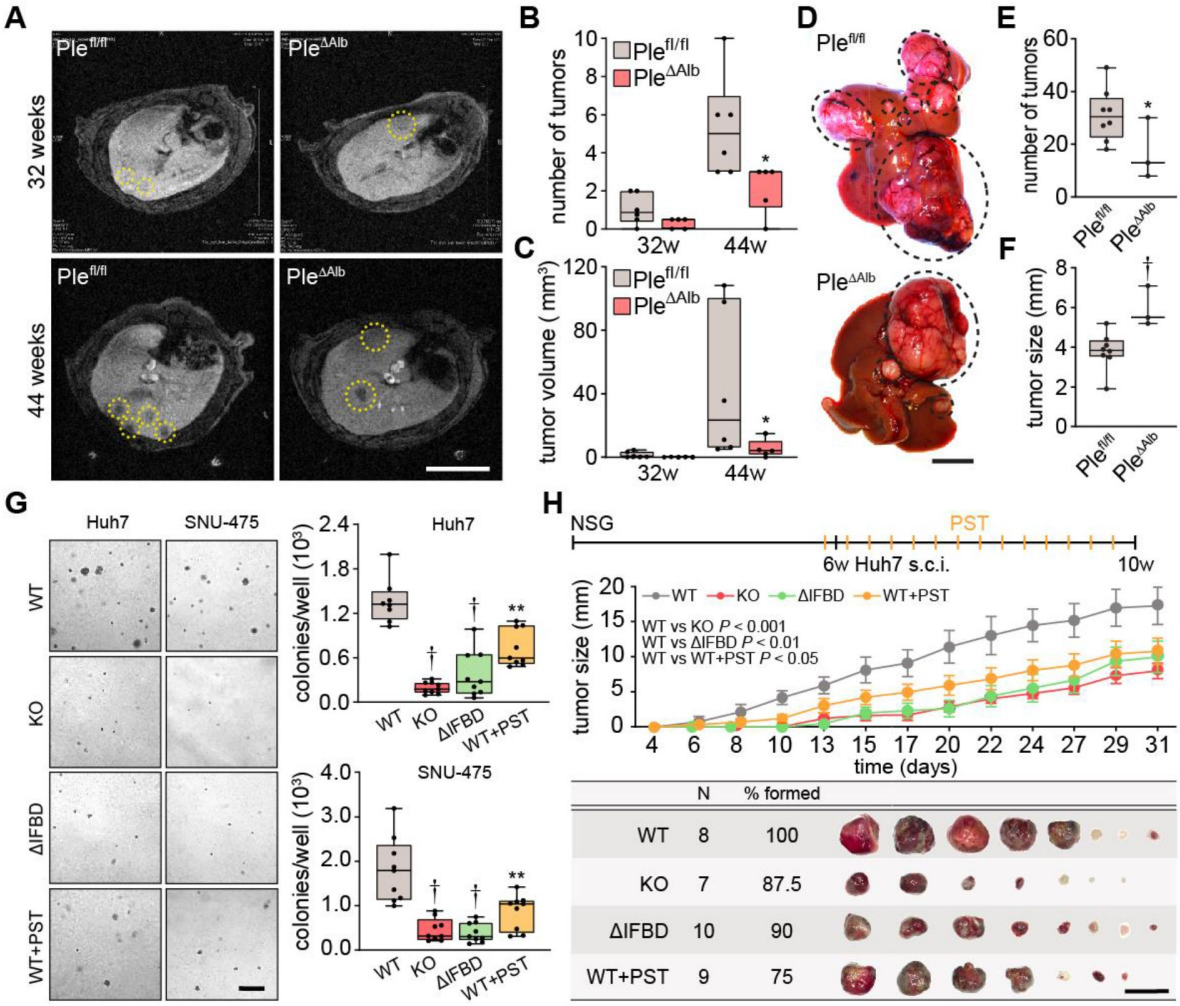

Figure 2.

Plectin promotes HCC growth.

(A) Representative MRI images of *Ple*$^{fl/fl}$ and *Ple*$^{\Delta Alb}$livers at 32 and 44 weeks post-DEN injection. Dashed circles, tumors. Scale bar, 500 µm. **(B, C)** Quantification of tumor number (B) and volume (C) in *Ple*$^{fl/fl}$ and *Ple*$^{\Delta Alb}$ livers shown in (A). Boxplot shows the median, 25th, and 75th percentile with whiskers reaching the last data point; dots, individual mice; *N* = 6 (*Ple*$^{fl/fl}$), 5 (*Ple*$^{\Delta Alb}$). Two-tailed *t*-test; **P* < 0.05. **(D)** Representative images of *Ple*$^{fl/fl}$ and *Ple*$^{\Delta Alb}$ livers at 44 weeks post-induction. Dashed circles, tumors. Scale bar, 1 cm. **(E, F)** Quantification of the number (E) and size (F) of *Ple*$^{fl/fl}$ and *Ple*$^{\Delta Alb}$ tumors shown in (D). Boxplot shows the median, 25th, and 75th percentile with whiskers reaching the last data point; dots, individual mice; *N* = 8 (*Ple*$^{fl/fl}$), 3 (*Ple*$^{\Delta Alb}$). Two-tailed *t*-test; **P* < 0.05; < 0.001. **(G)** Representative images of colonies from WT, KO, ΔIFBD, and PST-treated WT (WT+PST) Huh7 and SNU-475 cells grown in soft agar. Scale bar, 500 µm. Boxplots show the number of Huh7 (upper graph) and SNU-475 (lower graph) cell colonies. The box represents the median, 25th, and 75th percentile with whiskers reaching the last data point; dots, agar wells; *n* = 9 agar wells; *N* = 3. Two-tailed *t*-test; ***P* < 0.01; < 0.001. **(H)** Six-week-old NSG mice were subcutaneously injected with indicated Huh7 cells into both hind flanks and were kept either untreated (WT, KO, and ΔIFBD) or daily treated by orogastric gavage of plecstatin (WT+PST) as indicated in upper bar. Mice were sacrificed 4 weeks post-injection and xenografts were dissected. The graph shows the time course of xenograft growth. Data are shown as mean ± SEM; n = 8 (WT), 7 (KO), 10 (ΔIFBD) and 9 (WT+PST) tumors; *N* = 4 (WT), 4 (KO), 5 (ΔIFBD) and 6 (WT+PST). Two-way ANOVA. The table shows the number (N), percentage, and representative images of formed xenografts. Scale bar, 2 cm.

To further assess whether plectin is required for human HCC progression, we investigated the growth of subcutaneous Huh7 xenografts in immunodeficient NSG mice (**Fig. 2H**; **Figure 2**—figure supplement 1G). Cells with disabled plectin developed significantly smaller tumors when compared with untreated WT cells (**Fig. 2H**), mirroring the results of the colony forming assay. The percentage of $Ki67^+$ cells on immunolabeled xenograft sections, however, did not differ between experimental conditions (**Figure 2**—figure supplement 1G). These results show the reduced tumorigenic potential of human HCC cells when plectin is disabled either by CRISPR/Cas9-mediated gene ablation or pharmacologically with PST. Hence, by combining *in vivo* and *in vitro* approaches, we provide evidence that plectin promotes hepatocarcinogenesis.

Plectin controls oncogenic FAK, MAPK/Erk, and PI3K/Akt signaling in HCC cells

To identify potential molecular effectors and signaling pathways mediating the tumor suppressive effects of plectin inactivation, we profiled the proteomes of WT, KO, and PST-treated WT SNU-475 cells using MS-based shotgun proteomics and phosphoproteomics (**Fig. 3A-C**; **Figure 3**—figure supplement 1A,B). Using a label free quantification strategy, a total of 5440 protein groups and 3573 phosphosites were detected. We found 265 protein groups significantly regulated (FDR < 0.05; s0 = 0.01) upon plectin ablation when comparing WT and KO SNU-475 proteomes (**Fig. 3B**). Ingenuity Pathway Analysis (IPA) revealed major plectin-dependent regulation of signaling pathways related to the actin cytoskeleton, such as “RhoA signaling”, “Actin cytoskeleton signaling”, “Integrin signaling”, and “Signaling by Rho family GTPases” (**Fig. 3B**). Similarly, 313 regulated phosphosites indicated a major impact on actin, as well as “ILK signaling”, “FAK signaling”, and “Molecular mechanisms of cancer” among the most altered pathways (**Fig. 3B**).

Analysis of proteome differences between WT and PST-treated cells identified abundance changes (FDR < 0.05; s0 = 0.01) in 1178 proteins and 290 phosphoproteins (**Fig. 3C**). A comparison of KO and PST signatures using IPA revealed an overlap (**Figure 3**—figure supplement 1A). Consistently, the IPA annotation linked also PST signature to integrin- and cytoskeleton-related signaling pathways such as “ILK signaling”, “Integrin signaling”, “RhoA signaling”, and “Actin cytoskeleton signaling” (**Fig. 3C**). Taken together, our proteomic analyses suggest a regulatory role for plectin in the mechanosensitive, cell adhesion-linked signaling which is critical for cancer development and dissemination[3–5].

To independently confirm our MS findings, we performed extensive immunoblot analysis of WT, KO, ΔIFBD, and PST-treated Huh7 and SNU-475 cells with a focus on integrin-associated adhesome network (**Fig. 3D**; **Figure 3**—figure supplement 1C). In agreement with our proteomic analyses, plectin inactivation resulted in considerable changes in expression levels of integrin adhesion receptors (integrins αV and β1) as well as other FA constituents (i.e. talin, vinculin, and paxillin). Moreover, immunoblotting revealed in cells with disabled plectin either generally altered expression (FAK, AKT, Erk1/2, ILK, and PI3K) and/or reduced phosphorylation (AKT, Erk1/2, and PI3K) of key effectors downstream of integrin-mediated adhesion. Although these alterations were not found systematically in both cell lines and condition (reflecting thus presumably their distinct differentiation grade and plectin inactivation efficacy), collectively these data confirmed plectin-dependent adhesome remodeling together with attenuation of oncogenic FAK, MAPK/Erk, and PI3K/Akt pathways upon plectin inactivation (**Fig. 3E**).

Plectin-dependent disruption of cytoarchitecture accounts for hampered migration of HCC cells

As plectin acts as a major organizer of cytoskeletal networks[10], we next investigated cytoskeletal organization in HCC cells by immunofluorescence microscopy. To circumvent considerable variability in cellular morphology, which largely obscures quantitative assessment of cytoarchitecture, we seeded WT, KO, ΔIFBD, and PST-treated SNU-475 cells on crossbow-shaped

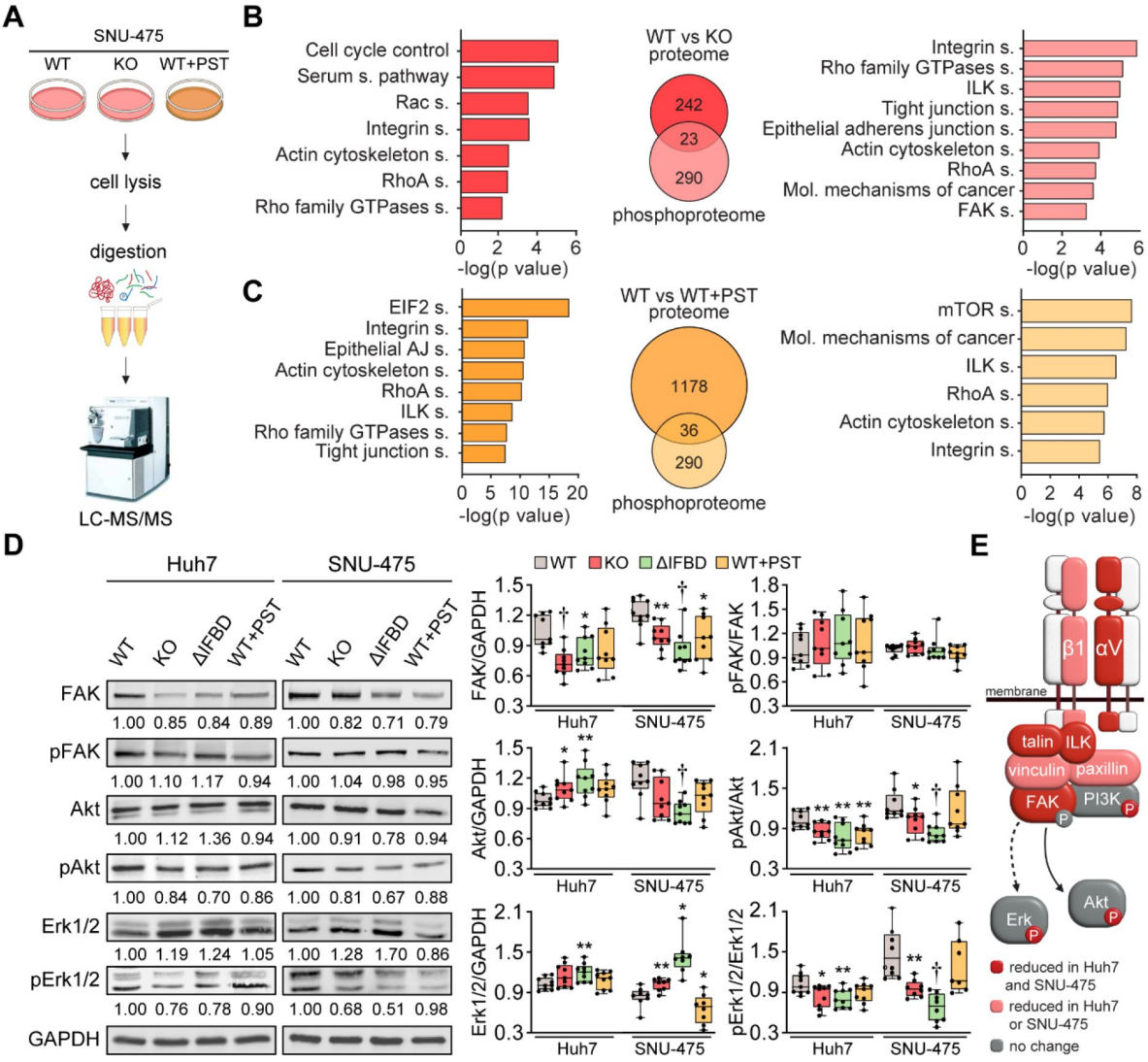

Figure 3.

CRISPR/Cas9- or PST-mediated plectin inactivation attenuates HCC oncogenic potential through FAK, Erk1/2, and PI3K/Akt axis.

(A) Schematic of MS-based proteomic analysis of WT, KO, and PST-treated WT (WT+PST) SNU-475 cells. **(B,C)** Ingenuity Pathway Analysis (IPA) canonical signaling pathways predicted from differentially expressed proteins identified by proteomics (left) and phosphoproteomics (right) in WT vs. KO (B) and WT vs. WT+PST (C) proteomes. Venn diagrams show relative proportions of differentially expressed proteins. Two-sided Student's *t*-test with multiple testing correction: FDR < 0.05; s0 = 0.1; triplicates. **(D)** Quantification of FAK, phospho-Tyr397-FAK (pFAK), Akt, phospho-Ser473-Akt (pAkt), Erk1/2, and phospho-Thr202/Tyr204-Erk (pErk) in indicated Huh7 and SNU-475 cell lines by immunoblotting. GAPDH, loading control. The numbers below lines indicate relative band intensities normalized to average WT values. Boxplots show relative band intensities normalized to GAPDH or non-phosphorylated protein. The box represents the median, 25th, and 75th percentile with whiskers reaching the last data point; dots, individual experiments; $N = 9$. Two-tailed *t*-test; $*P < 0.05$; $**P < 0.01$; < 0.001. **(E)** Schematic representation of immunoblot analyses of adhesome-associated signaling shown in (F) and (Extended Data Fig. 2h). Proteins with significantly reduced expression levels and/or phosphorylation status (P) upon plectin inactivation in both HCC cell lines are highlighted in red, proteins with significantly reduced expression levels upon plectin inactivation in either Huh7 or SNU-475 cells are highlighted in pink.

micropatterns[29]. Reminiscent of plectin-deficient fibroblasts[20,30], plectin inactivation in SNU-475 cells produced less delicate vimentin networks compared to WT cells, with filaments often bundled and sometimes collapsing into vimentin clumps (**Fig. 4A,B**). A quantitative analysis revealed uneven distribution of vimentin filaments throughout the cytoplasm of KO, ΔIFBD, and PST-treated WT cells as evidenced by the distance between the position of the center of vimentin intensity mass and the cell center (**Figure 4**—figure supplement 1A-C). In addition to the aberrant vimentin phenotype, we noticed a dramatic reduction in longitudinal dorsal actin stress fibers and transversal arcs, as well as pronounced ventral stress fibers in plectin-disabled cells (**Fig. 4A,C**,D). Moreover, we detected a reduction in F-actin fluorescence intensity in both Huh7 and SNU-475 KO cells, as well as a decrease of atomic force microscopy (AFM)-inferred cellular stiffness as a functional readout for a well-formed cytoskeleton[16]. (**Figure 4**—figure supplement 1D-G).

Given the extent of plectin-dependent adhesome remodeling (**Fig. 3D,E**; **Figure 3**—figure supplement 1C), we next assessed whether plectin inactivation affects the morphology and localization of FAs in vinculin-immunolabeled SNU-475 cells. Remarkably, while FAs of micropattern- seeded WT cells were mostly located at the cell periphery, FAs of plectin-disabled cells were frequently found within the cell interior (**Fig. 4A,E**). Moreover, plectin inactivation resulted in an overall reduced number of FAs, and the FAs that remained were larger and more elongated than in WT cells (**Fig. 4F,G**; **Figure 4**—figure supplement 1H,I). To test whether the changes in actin/FA configuration affected adhesion-transmitted forces, we performed traction force microscopy (TFM; **Fig. 4H,I**). The smaller FAs found in WT cells transmitted significantly higher contractile energy than KO, ΔIFBD, and PST- treated cells, indicating that FAs in plectin-deficient cells were less functional than in WT.

Functional transmission of actomyosin-generated forces across FAs constitutes a prerequisite for cellular locomotion[31]. Therefore, we examined the effect of plectin inactivation on the migration of HCC cells. As anticipated, both Huh7 and SNU-475 cells exhibited a decrease in migration speed upon plectin targeting in the scratch wound healing assay (**Fig. 5A,B**; **Figure 5**—figure supplement 1A). It is noteworthy that migrating plectin-disabled SNU-475 cells exhibited more cohesive, epithelial-like features while progressing collectively. By contrast, WT SNU-475 leader cells were more polarized and found to migrate into scratch areas more frequently than their plectin-deficient counterparts (**Figure 5**—figure supplement 1B). Consistent with this observation, individually seeded SNU-475 cells less frequently assumed a polarized, mesenchymal-like shape upon plectin inactivation in both 2D and 3D environments (**Fig. 5C**). Moreover, plectin-inactivated SNU-475 cells exhibited a decrease in N- cadherin and vimentin levels when compared to WT counterparts (**Figure 5**—figure supplement 1C).

In addition to slower general migration, we also found epithelial growth factor (EGF)-guided migration potential of individual KO, ΔIFBD, and PST-treated cells to be significantly reduced compared to WT cells. Consistent with previous findings[20], plectin-disabled cells traversed less linear trajectories in both random and directed scenarios (**Fig. 5D,E**; **Figure 5**—figure supplement 1D,E). To determine whether plectin is involved in migration-associated cellular shape dynamics, we further investigated protrusions of SNU-475 cells using morphodynamic contour analysis[32]. Our analysis revealed a higher protrusion frequency of randomly migrating WT compared to plectin-disabled cells (**Figure 5**—figure supplement 1F), while no differences in protrusion orientation were observed (**Fig. 5F-H**). In sharp contrast, plectin ablation dramatically reduced the capacity of KO and ΔIFBD cells to form stable protrusions in the direction of chemotactic motion (**Fig. 5F-H**), although only a marginal effect on the protrusivity was observed (**Figure 5**—figure supplement 1F). Collectively, these results show that plectin is essential for the proper cytoskeletal configuration of HCC cells and their cytoskeleton-linked FAs. Moreover, they provide evidence that aberrant cytoarchitecture of plectin-disabled cells accounts for the failure to effectively exert traction forces and actively reconfigure body shape, both of which are required for HCC cell migration.

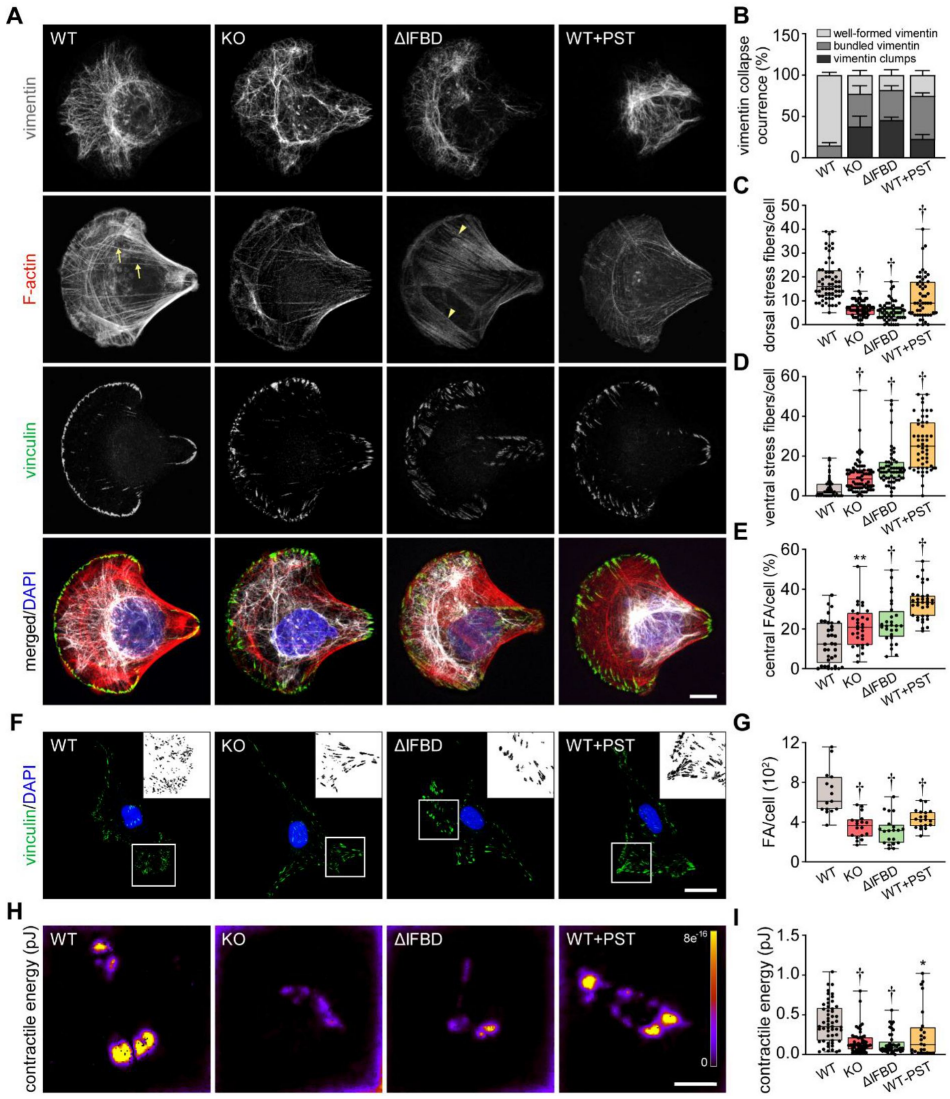

Figure 4.

Disruption of cytoskeletal networks upon plectin inactivation accounts for reduced contractility and aberrant adhesions in HCC cells.

(A) Representative confocal images of crossbow- shaped fibronectin micropattern-seeded WT, KO, ΔIFBD, and PST-treated WT (WT+PST) SNU-475 cells stained for F-actin (red), vinculin (green), and vimentin (grey). Nuclei, DAPI (blue). Arrows, dorsal stress fibers; arrowheads, ventral stress fibers. Scale bar, 10 µm. **(B)** Quantification of the percentage of cells (shown in (A)) with well-formed, bundled, and clump-containing vimentin networks. Data are shown as mean ± SEM; *n* = 60 (WT), 68 (KO), 55 (ΔIFBD), 50 (WT+PST) cells; *N* = 4 (WT, KO, IFBD), 3 (WT+PST). **(C,D)** Quantification of the number of dorsal (C) and ventral (D) actin stress fibers in cells shown in (A). Boxplots show the median, 25th, and 75th percentile with whiskers reaching the last data point; dots, individual cells; *n* = 60 (WT), 68 (KO), 55 (ΔIFBD), 50 (WT+PST); *N* = 4 (WT, KO, IFBD), 3 (WT+PST). Two-tailed *t*-test; < 0.001. **(E)** Quantification of FAs located within the interior of cells (central) shown in (A). Boxplot shows the median, 25th and 75th percentile with whiskers reaching the last data point; dots, individual cells; *n* = 25 (WT), 26 (KO), 23 (ΔIFBD), 28 (WT+PST); *N* = 3. ***P* < 0.01; < 0.001. **(F)** Representative confocal images of WT, KO, ΔIFBD, and PST-treated WT (WT+PST) SNU-475 cells immunolabeled for vinculin (green). Nuclei, DAPI (blue). Boxed areas, representative FA clusters shown as segmented binary maps in x2 enlarged insets. Scale bar, 30 µm. **(G)** Quantification of FA number in cells shown in (F). Boxplot shows the median, 25th, and 75th percentile with whiskers reaching the last data point; dots, individual cells; *n* = 15 (WT), 18 (KO), 20 (ΔIFBD), 19 (WT+PST); *N* = 3. Two-tailed *t*-test; < 0.001. **(H)** Pseudocolor spatial maps of contractile energy determined by TFM in WT, KO, ΔIFBD, and PST-treated WT (WT+PST) SNU-475 cells. Scale bar, 50 µm. **(I)** Quantification of contractile energy in cells shown in (H). Boxplots show the median, 25th, and 75th percentile with whiskers reaching the last data point; dots, individual cells; *n* = 54 (WT), 53 (KO), 41 (ΔIFBD), 24 (WT+PST) cells; *N* = 4. Two-tailed *t* test; **P* < 0.05; ***P* < 0.01; < 0.001.

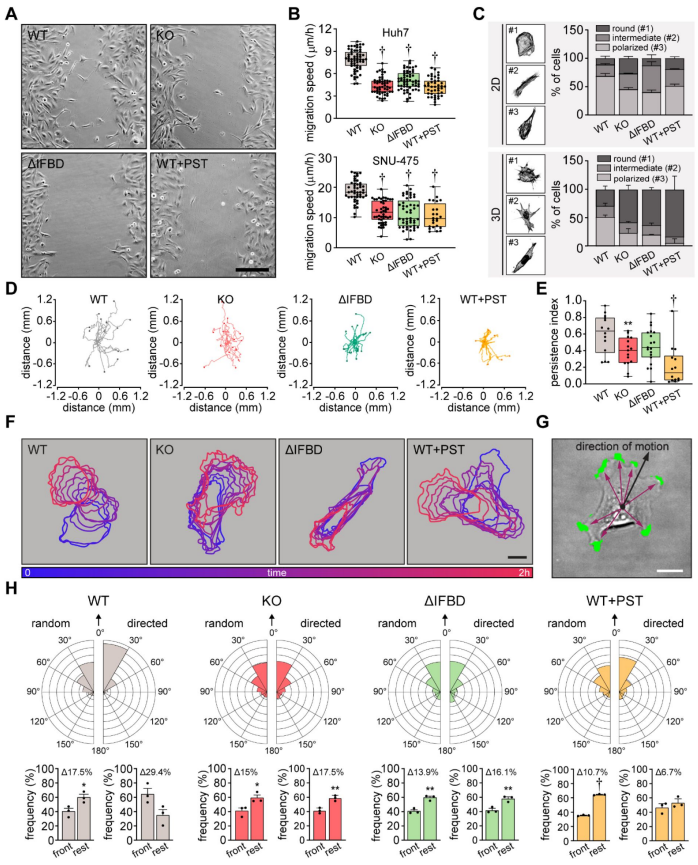

Figure 5.

Plectin links migration potential of HCC cells to cell shape dynamics.

(A) Representative phase contrast images of WT, KO, ΔIFBD, and PST-treated WT (WT+PST) SNU-475 cells migrating in the scratch-wound assay for 14 hours. Note individual, highly polarized WT cells frequently migrating into scratch areas. Scale bar, 200 µm. **(B)** Quantification of migration speed of indicated Huh7 (upper graph) and SNU-475 (lower graph) cells. Boxplots show the median, 25th, and 75th percentile with whiskers reaching the last data point; dots, fields of view; *n* (Huh7) = 59 (WT), 51 (KO), 58 (ΔIFBD), 43 (WT+PST); *n* (SNU-475) = 47 (WT), 47 (KO), 50 (ΔIFBD), 24 (WT+PST); *N* (Huh7) = 3; *N* (SNU-475) = 5 (WT, KO, ΔIFBD), 3 (WT+PST). Two-tailed *t*-test; $P < 0.001$. **(C)** Representative confocal images of F- actin stained WT, KO, ΔIFBD, and PST-treated WT (WT+PST) SNU-475 cells grown on fibronectin- coated coverslips (2D) or in collagen (3D) and classified as round (#1), intermediate (#2), and polarized (#3) shape. Quantification of the percentage of cell shape categories in indicated 2D and 3D SNU-475 cell cultures. Data are shown as mean ± SEM; *N* (2D) = 3; *N* (3D) = 5 (WT), 3 (KO, ΔIFBD), 2 (WT+PST). **(D)** Spider plots with migration trajectories of WT, KO, ΔIFBD, and PST-treated WT (WT+PST) SNU-475 cells tracked during 16 hours of EGF-guided migration; dots, the final position of each single tracked cell. **(E)** Quantification of processivity indices of WT, KO, ΔIFBD, and PST-treated WT (WT+PST) SNU- 475 cells. Boxplot shows the median, 25th, and 75th percentile with whiskers reaching the last data point; dots, individual cells; *n* = 15 (WT), 15 (KO), 19 (ΔIFBD), 14 (WT+PST); *N* = 3. Two-tailed *t*-test; $^{**}P < 0.01$; $P < 0.001$. **(F)** Representative time sequences of the WT, KO, ΔIFBD, and PST-treated WT (WT+PST) SNU-475 cell contours during EGF-guided migration. Color coding indicates the time of cell position acquired in 10-minute intervals. Scale bar, 20 µm. **(G)** Representative phase contrast image of SNU-475 cell with protrusions (green) segmented from superimposed contours used in morphodynamic analysis. Extension vectors (purple arrows) were drawn from the center of the cell nucleus towards individual protrusions and related to the direction of cell motion (black arrow). Scale bar, 20 µm. **(H)** Rose graphs show the percentage of extension vector directions in 30° cones, normalized to the directions of random and EGF-guided (directed) motions (0°; arrows) of WT, KO, ΔIFBD, and PST-treated WT (WT+PST) SNU-475 cells. *n* = 9752 extensions in 22 cells (WT random), 4167 extensions in 15 cells (WT directed), 8394 extensions in 19 cells (KO random), 5107 extensions in 15 cells (KO directed), 8362 extensions in 21 cells (ΔIFBD random), 5809 extensions in 19 cells (ΔIFBD directed), 9450 extensions in 20 cells (WT+PST random), 4350 extensions in 14 cells (WT+PST directed); *N* = 3. Bar graphs show the percentage of cell extensions formed either in the direction of motion (frontal, 30° to -30° cones) or along the rest of the cell perimeter (rest). Data are shown as mean ± SEM; dots, biological replicates; *N* = 3. Two-tailed *t*-test; $^{*}P < 0.05$; $^{**}P < 0.01$; $P < 0.001$.

Plectin inactivation reduces HCC cell invasion and lung colonization

To investigate whether disruption of cytoarchitecture in plectin-disabled HCC cells also affected 3D migratory behavior, we compared the activity of WT, KO, ΔIFBD, and PST-treated SNU-475 cells in transwell and spheroid invasion assays. In both assays, plectin inactivation significantly reduced invasion potential compared to WT cells (**Fig. 6A-C**; **Figure 6**—figure supplement 1A). Unexpectedly, plectin-targeted cells also degraded dramatically less FITC-labeled gelatin, suggesting that slower invasion is accompanied by defects in ECM degradation (**Fig. 6D**; **Figure 6**—figure supplement 1B).

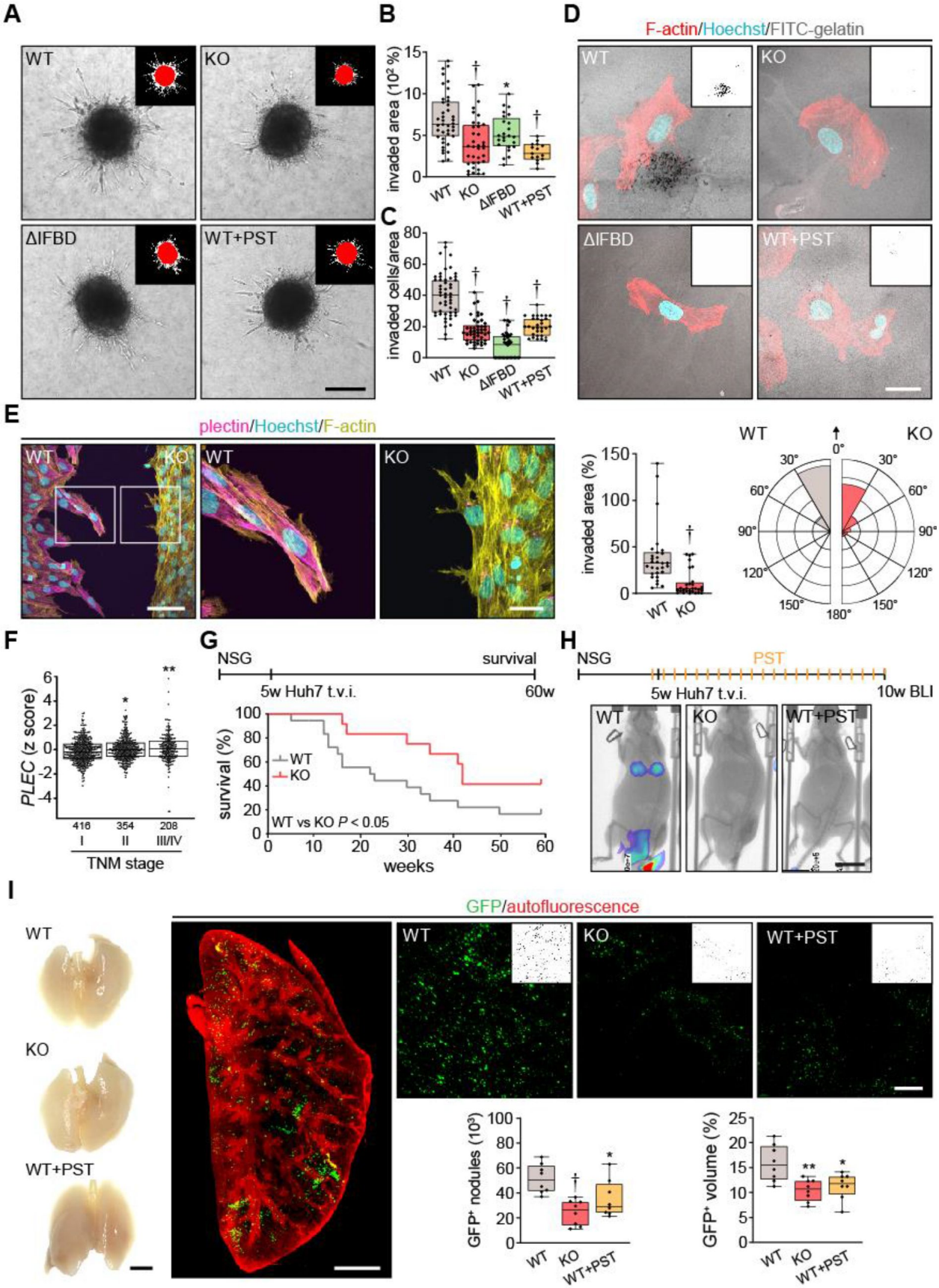
A
WT
KO
ΔIFBD
WT+PST
B
invaded area (10² %)
C
invaded cells/area
D
F-actin/Hoechst/FITC-gelatin
E
plectin/Hoechst/F-actin
invaded area (%)
F
PLEC (z score)
TNM stage
G
NSG
survival
5w Huh7 t.v.i.
60w
survival (%)
WT vs KO P < 0.05
weeks
H
PST
10w BLI
I
GFP/autofluorescence
GFP⁺ nodules (10³)
GFP⁺ volume (%)

Figure 6.

Plectin inactivation inhibits HCC invasion and metastasis.

(A) Representative images of WT, KO, ΔIFBD, and PST-treated WT (WT+PST) SNU-475 spheroids grown for 3 days in collagen mixture. Insets, superimposed binary masks of initial (red) and final (white) spheroid area. Scale bar, 200 µm. **(B)** Quantification of the invaded area calculated as the percentage of the initial spheroid area from day 0. Boxplots show the median, 25th, and 75th percentile with whiskers reaching the last data point; dots, individual spheroids; *n* = 47 (WT), 44 (KO), 34 (ΔIFBD), 25 (WT+PST) spheroids; *N* = 5 (WT, KO), 4 (ΔIFBD), 3 (WT+PST). Two-tailed *t*-test; ***P* < 0.01; < 0.001. **(C)** Quantification of the number of indicated cells invaded in Matrigel transwell assay. Boxplots show the median, 25th, and 75th percentile with whiskers reaching the last data point; dots, fields of view; *n* = 51 (WT), 45 (KO), 38 (ΔIFBD), 31 (WT+PST) fields of view; *N* = 4 (WT, KO), 3 (ΔIFBD, WT+PST). Two-tailed *t*-test; < 0.001. **(D)** Representative confocal micrographs of WT, KO, ΔIFBD, and PST-treated WT (WT+PST) SNU-475 cells grown on FITC-labeled gelatin (grey) for 24 hours and stained for F-actin (red). Nuclei, Hoechst (blue). Insets, segmented binary masks of FITC-gelatin signal. Black regions correspond to gelatin areas degraded by individual cells. Scale bar, 30 µm. **(E)** Representative confocal images of WT and KO SNU- 475 cells during the Matrigel invasion assay, stained for plectin (magenta) and F-actin (yellow). Nuclei, Hoechst (blue). See Video 1. Boxed areas, x3 images. Scale bars, 100 and 30 µm (boxed areas). Boxplot shows the invaded area calculated as the percentage of the initial area covered by WT and KO cells. The box represents the median, 25th, and 75th percentile with whiskers reaching the last data point; dots, fields of view; *n* = 29 fields of view; *N* = 2. Rose graphs show the percentage of extension vector directions in 30° cones, normalized to the directions of cell motions (0°; arrow) during matrigel invasion. *n* = 857 extensions in 18 cells (WT), 623 extensions in 12 cells (KO); *N* = 2. Two-tailed *t*-test; < 0.001. **(F)** Relative *plectin* (*PLEC*) mRNA expression in samples collected from HCC patient meta- cohort clustered based on TNM classification (stage I-IV). The meta-cohort includes 6 different datasets from 5 platforms (for details, see Materials and methods section). The numbers of participants per stage are indicated in the graph. Scattered boxplots show individual data points, median, 25th, and 75th percentile; *N* = 978. Wilcoxon rank-sum test; **P* < 0.05; ***P* < 0.01. **(G)** The 5- week-old NSG mice were injected (t.v.i.) with WT and KO RedFLuc-GFP-expressing Huh7 cells generated for lung colonization assay. Kaplan-Meier curves show the overall survival of mice injected with the cells indicated. *N* = 14 (WT), 13 (KO). Long-rank test, *P* < 0.05. **(H)** The 5-week-old NSG mice were injected (t.v.i.) with indicated RedFLuc-GFP-expressing Huh7 cells. WT cell-bearing mice were kept either untreated or every second day provided with orogastric gavage of plecstatin (WT+PST) as indicated. Five weeks post-injection mice were screened by whole-body bioluminescence imaging (BLI). Representative BLI images of WT, KO, and PST-treated WT (WT+PST) Huh7 cells-bearing mice are shown. Scale bar, 2 cm. **(I)** Representative images of lungs dissected from mice shown in (H). Scale bar, 1 cm. Representative lattice light sheet fluorescence image of clear, unobstructed brain imaging cocktails (CUBIC)-cleared lung lobe immunolabeled with antibodies against GFP (green). Autofluorescence visualizing the lobe structures is shown in red. Scale bar, 2 mm. Representative magnified images from lung lobes with GFP-positive WT, KO, and WT+PST Huh7 nodules. Insets, segmented binary masks of GFP-positive metastatic nodules. Scale bar, 400 µm. Boxplots show metastatic load in the lungs expressed as the number (left graph) and relative volume (right graph) of indicated GFP-positive (GFP^+) nodules. The box represents the median, 25th, and 75th percentile with whiskers reaching the last data point; dots, lung lobes; *n* = 8 lung lobes; *N* = 4. Two-tailed *t*-test; **P* < 0.05; ***P* < 0.01; < 0.001.

To monitor plectin effects on shape dynamics in a 3D environment, we recorded WT and KO SNU-475 cells by time-lapse video microscopy in a matrigel invasion assay. Invading WT cells exhibited polarized protrusions followed by cell body displacement in the direction of the nascent protrusion (Video 1; **Fig. 6E**). By contrast, randomly oriented thinner protrusions of KO cells were often retracted shortly after formation. Markedly thinner and branched KO protrusions were confirmed by subsequent immunofluorescence microscopy (**Fig. 6E**). Similar to what we observed in the 2D assay, KO cells failed to invade in the direction of these transient protrusions (Video 1; **Fig. 6E**). Hence, plectin-controlled cytoarchitecture facilitates both 2D and 3D HCC cell migration.

Tumor, node, metastasis (TNM) classification of an HCC meta-cohort with clinically annotated tumors from HCC patients (n = 978) demonstrated that high plectin mRNA expression is associated with advanced TNM stages (**Fig. 6F**). To elucidate the impact of plectin inactivation on HCC dissemination, we conducted the lung colonization assay using both Huh7 and SNU-475 cells (**Fig. 6G** - I; **Figure 6**—figure supplement 1C-F). To this end, we administered red firefly luciferase and GFP (RedFLuc-GFP)-expressing WT and KO cells intravenously (i.v.) in 5-week-old NSG mice. Whereas mice receiving WT Huh7 (but not SNU-475; data not shown) cells succumbed rapidly to disease, mice receiving KO cells exhibited prolonged survival (**Fig. 6G**). To identify early phase of metastasis formation, we next monitored the HCC cell retention in the lungs using *in vivo* bioluminescence imaging (**Fig. 6H**). This experimental cohort was expanded for WT-injected mice which were administered PST two times a day for 5 weeks (WT+PST). Mice were sacrificed 5 weeks post-injection when the first luminescence-positive chest areas were detected (**Fig. 6H**) and cleared whole lung lobes were analyzed by lattice light sheet fluorescence microscopy (**Fig. 6I**). Although no macroscopic Huh7 nodules were visible, we found a prominent reduction in the number and volume of GFP-positive KO- and WT+PST-derived metastatic nodules. Thus, both CRISPR/Cas9-based and pharmacological plectin inactivation in HCC potently inhibits metastatic load in the lungs, identifying plectin as a potential target against tumor dissemination *in vivo*.

Genetic and pharmacological plectin targeting prevents hepatocarcinogenesis through signatures shared by animal models and patients

To further investigate the translational potential of PST treatment, we evaluated the effects of PST administration on hepatocarcinogenesis in additional murine model. To this end, we induced multifocal HCC tumors by hydrodynamic delivery of a *c-myc* (Myc)-encoding element together with a CRISPR/Cas9 construct targeting *Tp53* (sgTp53)[33]. To test whether HCC onset and progression are sensitive to pharmacological targeting of plectin, we monitored Myc;sgTp53-driven tumor development in $Ple^{fl/fl}$, $Ple^{\Delta Alb}$, and PST-treated $Ple^{fl/fl}$ male mice using MRI (**Fig. 7A**). Consistent with our *in vitro* observations, MRI analysis at 4, 6, and 9 weeks post-induction revealed that both genetic and pharmacological plectin inactivation results in a substantial reduction in the average tumor number per mouse and the tumor incidence (**Fig. 7A**). Stalled development of $Ple^{\Delta Alb}$and PST-treated $Ple^{fl/fl}$ tumors was also reflected by a decrease in liver/body weight ratio in another male cohort sacrificed at 6 weeks post-induction (**Fig. 7B,C**). The quantitative immunofluorescence microscopy revealed comparable rates of proliferation and apoptosis in Myc;sgTp53-induced tumors across experimental conditions (**Figure 7**—figure supplement 1A,B). Comparable trends in liver/body weight ratio and tumor incidence were also found in a female cohort sacrificed 8 weeks post-induction (**Figure 7**—figure supplement 1C,D).

To better understand the antitumor effects observed in PST-treated mice, we performed proteomics on Myc;sgTp53-treated $Ple^{fl/fl}$, $Ple^{\Delta Alb}$, and PST-treated $Ple^{fl/fl}$ livers. Consistent with (phospho)proteomic and immunoblot analyses of HCC cell lines (**Fig. 3A-E**) we found a high level of similarity between $Ple^{\Delta Alb}$ and PST-treated $Ple^{fl/fl}$ signatures (**Fig. 7D**; **Figure 7**—figure supplement 2A,B). In addition, gene set enrichment analysis (GSEA)[34] revealed enrichment in “PI3K/Akt” or “Hippo/YAP signaling” pathways (**Fig. 7D**). Although the data from liver tissue proteomics showed some degree of variation, enrichment of tension-dependent signatures points toward similar trends found in *in vitro* scenarios. To further translate our findings to the human setting, we correlated plectin transcript levels with differentially expressed signatures identified in proteomic analysis of HCC cells (**Fig. 3B-D**). Through analysis of 1268 HCC patients, we found gene sets annotated as “Integrin pathway”, “FAK pathway”, “PI3K Akt/mTOR signaling” or “Erk pathway” to positively correlate with elevated plectin expression (**Fig. 7E**; **Figure 7**—figure supplement 2C; **Figure 7**—figure supplement 3). Collectively, these data connect plectin with well-characterized pro-oncogenic signaling pathways which were previously identified as prime candidates for therapeutic intervention in cancer[3–5].

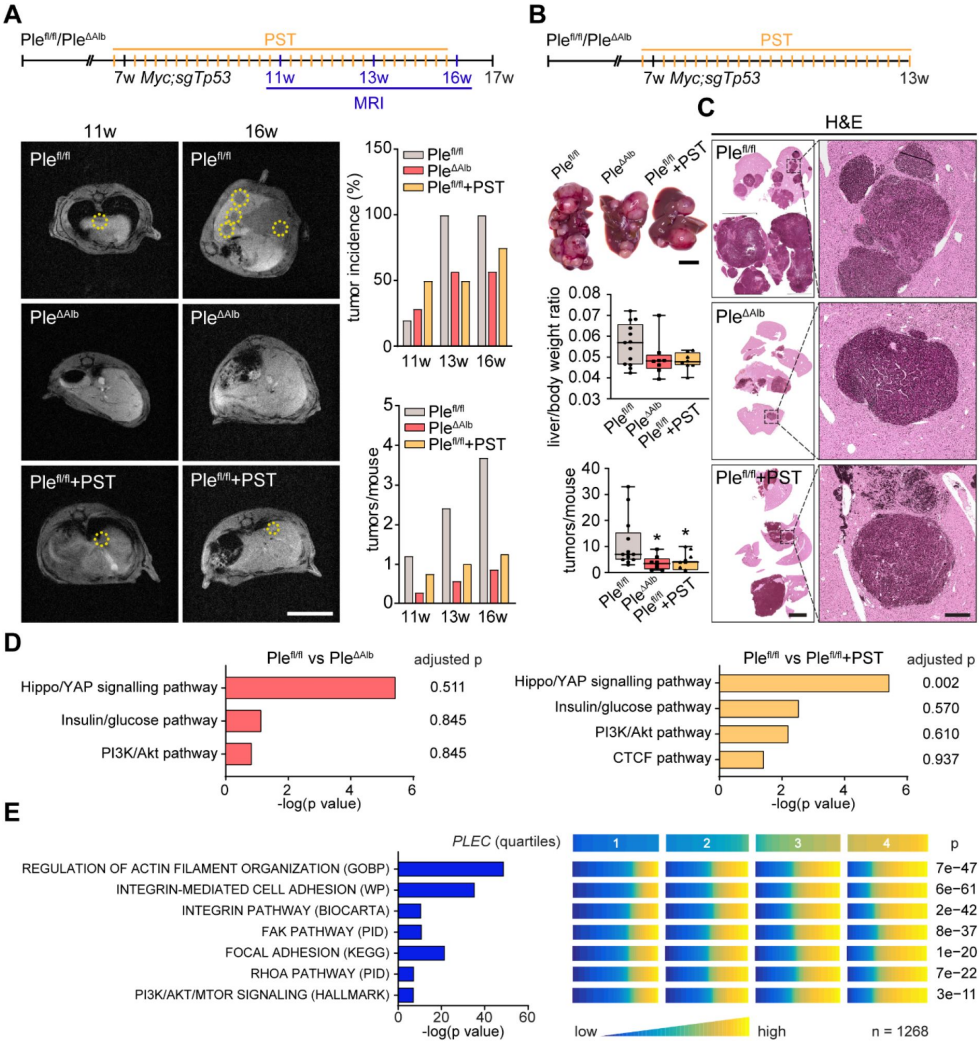

Figure 7.

Genetic and pharmacological plectin targeting prevents hepatocarcinogenesis through signatures shared by animal models and patients.

(A) HCC-predisposing lesions were introduced by hydrodynamic gene delivery via tail vein injection (HDTVi) of transposon vector encoding cMyc in conjunction with CRISPR/Cas9 construct targeting *Tp53* (Myc;sgTp53) in $Ple^{fl/fl}$ and $Ple^{\Delta Alb}$ cohorts of 7- week-old male mice. $Ple^{fl/fl}$ mice were kept either untreated or every second day provided with orogastric gavage of plecstatin ($Ple^{fl/fl}$+PST) and the development of HCC was monitored by MRI at 11, 13, and 16 week, as indicated. Representative MRI images of $Ple^{fl/fl}$ and $Ple^{\Delta Alb}$ and $Ple^{fl/fl}$+PST tumors acquired at indicated time points. Dashed circles, tumors. Scale bar, 2 cm. Graphs show the average number of tumors (lower graph) and percentual tumor incidence (upper graph) inferred from MRI images. *N* = 5 ($Ple^{fl/fl}$), 7 ($Ple^{\Delta Alb}$), 4 ($Ple^{fl/fl}$+PST). **(B)** Myc;sgTp53 HCC was induced in $Ple^{fl/fl}$, $Ple^{\Delta Alb}$, and PST-treated $Ple^{fl/fl}$ ($Ple^{fl/fl}$+PST) male mice as in (A). Shown are representative images of $Ple^{fl/fl}$, $Ple^{\Delta Alb}$, and $Ple^{fl/fl}$+PST livers from mice with fully developed multifocal HCC sacrificed 6 weeks post-induction. Scale bar, 1 cm. Boxplots show tumor burden in the livers expressed as the liver/body weight ratio (upper graph) and number of tumors per mouse (lower graph). The box represents the median, 25th, and 75th percentile with whiskers reaching the last data point; dots, mice; *N* = 12 ($Ple^{fl/fl}$), 9 ($Ple^{\Delta Alb}$), 10 ($Ple^{fl/fl}$+PST). Two-tailed *t*-test; *$P < 0.05$. **(C)** Representative images of H&E-stained $Ple^{fl/fl}$, $Ple^{\Delta alb}$, and $Ple^{fl/fl}$+PST liver sections. Note darker areas corresponding to HCC lesions. Boxed areas, x12 images. Scale bars, 5 and 1 mm (boxed areas). **(D)** Gene set enrichment analysis of differentially regulated proteins in $Ple^{fl/fl}$ vs $Ple^{\Delta Alb}$ and $Ple^{fl/fl}$vs $Ple^{fl/fl}$ + PST livers from the cohort shown in (A). Prediction of canonical signaling pathways in $Ple^{fl/fl}$ vs $Ple^{\Delta Alb}$ (left) and $Ple^{fl/fl}$vs $Ple^{fl/fl}$ + PST (right) proteomes. **(E)** Association of plectin-dependent signatures compiled from human HCC-derived cells (see **Fig. 3B-E**) and mouse models (see **Fig. 7D**) with *plectin* (*PLEC*) mRNA expression in HCC patients. Right panel shows the levels of selected signatures in patients grouped into quartiles of *PLEC* expression level. *N* = 1268. *P* values were generated from an analysis of variance (ANOVA).

Discussion

HCC represents a leading cause of cancer-related death, characterized by poor long-term prognosis, high postoperative recurrence, and a high rate of metastasis[35,36]. As chemotherapy, surgical resection, radiation, and local ablation are not effective in a large group of patients[35,37], there is an urgent need to develop effective therapeutic strategies to target HCC. By combining comprehensive analysis of CRISPR/Cas9-engineered HCC cell lines with (phospho)proteomics, mouse modeling as well as human patient data, we identified the plakin family member plectin as a novel HCC marker and druggable target upstream of FAK, MAPK/Erk, and PI3K/AKT signaling. Thus, our data link plectin, a cytolinker implicated in cytoskeletal tension and mechanotransduction with a major oncogenic signaling hub controlling growth and metastasis of HCC.

We began this work by assessing plectin expression in publicly available HCC patient datasets. Our meta-analyses revealed plectin transcript levels to be considerably elevated in HCC irrespective of etiology or gender, whereas previous findings in HCC were inconsistent[11,38]. Notably, we found that patients with higher *PLEC* mRNA levels had significantly shorter recurrence-free survival times than those with lower *PLEC* mRNA levels. Strikingly, *PLEC* expression in publicly available datasets was significantly associated with gene signatures related to „cell survival and proliferation“, „angiogenesis“, and „hypoxia“ (**Figure 7**—figure supplement 3) indicating that the *PLEC* level was associated with more aggressive cancer traits in HCC patients. In addition, plectin expression levels were associated with TNM staging, underscoring plectińs prognostic value for HCC patient survival. Although HCC transcriptomes appears to differ from other cancers[39], our findings are in line with higher *PLEC* expression in other cancer entities such as oral squamous cell carcinoma[40,41], testicular cancer[42], or pancreatic cancer[43], and identify plectin as a specific marker for both early and advanced stages of HCC.

We and others have proposed that plectin plays a central role in tumor growth and dissemination[12,44]. Here, using liver-specific $Ple^{\Delta Alb}$ knockout mice[26], we show that plectin ablation in hepatocytes significantly reduced tumor burden in a model of DEN-induced HCC[45], which mimics fundamental aspects of human disease[46]. These mice also showed decreased hepatocarcinogenesis in a powerful model of multifocal HCC formation following hydrodynamic delivery of Myc;sgTp53[33,47]. In this model, both genetic and PST-mediated pharmacological inactivation of plectin not only reduced the number of HCC tumors formed but ultimately resulted in significantly improved survival of $Ple^{\Delta Alb}$ female mice. Complementing the data from both HCC models, we found that plectin inactivation resulted in the reduced tumorigenic potential of human HCC cells, as evidenced by reduced colony growth under adhesion-independent conditions or subcutaneous xenografts in immunodeficient NSG mice. While several approaches (such as genetic manipulation[48], PST treatment[28] or blocking peptides[49] and antibodies[50]) decreasing the levels of functional plectin also lead to limited xenograft growth, to our knowledge, this is the first study showing that plectin inactivation prevents tumor progression in well-established preclinical mouse models.

Our previous studies demonstrated that plectin inactivation abrogates physical crosstalk between actin and IF networks[18,20], leading to the redistribution of internal tension[18], and ultimately resulting in defects in cell adhesions[20]. Indeed, plectin-dependent cytoskeletal disruption and aberrant adhesions have been previously linked to compromised migration and invasion of many non- cancerous[19,20,22,51,52] as well as cancerous cell types[48,53–56], including HCC cells[27]. In support of this concept, we report the collapse of actin and vimentin IF networks in Huh7 and SNU-475 cells with disabled plectin. Cytoskeletal disruption was accompanied by redistribution of misshapen FAs, which exerted reduced traction forces onto the underlying substrates. As anticipated, aberrant cytoarchitecture resulted in significantly slower

motility of HCC cells in both 2D and 3D environments. Consistent with *in vitro* findings, plectin inactivation reduced metastatic outgrowth of HCC cells in the lung. Intriguingly, morphodynamic contour analysis revealed in these cells reduced capacity to form stable protrusions implicated in driving path finding and cellular locomotion[31]. Collectively, our data suggest that plectin is essential for spatiotemporal cytoskeletal rearrangement, cell shape stabilization, and effective transmission of traction forces, and place plectin-mediated cytoskeletal crosstalk at the center of the processes that control the metastatic cascade.

Plectin-mediated cytoskeletal crosstalk at FAs facilitates their essential features such as dynamics[20], adhesion strength[57], and mechanotransduction capacity[20]. Loss of vimentin filament-FA linkage upon plectin deletion in highly migratory dermal fibroblasts was shown to uncouple the activation of FAK from actomyosin-generated tension and attenuate downstream effectors such as Src, Erk1/2, and p38[20]. Here we show that plectin-dependent perturbation of the cytoskeleton-FAs interplay in invasive SNU-475 HCC cells profoundly altered (phospho)proteomic signatures of cytoskeleton- and cell adhesion-annotated proteins, thereby modulating mechanosensitive integrin- associated signaling events. Importantly, our (phospho)proteomic and immunoblot analyses identified attenuated signaling along FAK, MAPK/Erk, and PI3K/Akt axes as a consequence of plectin inactivation in both Huh7 and SNU-475 HCC cells. Plectiṅs control of cytoskeletal crosstalk and its interplay with pro-oncogenic signaling pathways thus emerges as a critical determinant of the initiation and progression of HCC. It is noteworthy that plectin-dependent effects on PI3K/Akt and FAK/Erk signaling were recently described for prostate cancer[53,56] and head and neck squamous carcinoma cells[58], indicating that these observations have broader implications beyond liver cancer.

Finally, we were able to translate our findings from HCC cell lines and mouse models to HCC patients. By mining data from a large human patient cohort, we found a positive correlation between plectin expression and FA-associated FAK, Erk, and PI3K/Akt pathway gene sets. However, it is conceivable that dysregulated cytoskeletal crosstalk could affect HCC through multiple mechanisms independent from FA-associated signaling. Indeed, we and others[26,27] have shown that upon plectin inactivation, liver cells acquire epithelial characteristics that promote increased intercellular cohesion and reduced migration. Further studies will be required to identify and investigate synergistic adhesion- independent effects of plectin inactivation on HCC growth and metastasis.

Current systemic therapies for advanced HCC rely on a combination of multikinase inhibitors (such as sorafenib) or anti-VEGF /VEGF inhibitor (such as bevacizumab) treatment with immunotherapy[59]. Multikinase inhibitors provide only moderate survival benefit[60,61] due to primary resistance and the plasticity of signaling networks[62], and only a subset of patients benefits from addition of immunotherapy in HCC treatment[63]. Therefore, the most translationally impactful finding of this work is the ability of a small organoruthenium compound PST, a high-affinity plectin ligand, to effectivelly limit hepatocarcinogenesis in Myc;sgTp53-driven HCC mouse model as well as xenografted human HCCs, leading to the dampening of HCC burden. Using PST, we further report a marked effect on metastatic HCC outgrowth in the lung along with a reduction of the migratory potential of human HCC cells in 2D and 3D settings. Most notably, our animal models show improvement in local and metastatic survival rates. Similar to other ruthenium-based metallodrugs[64–66], PST was well-tolerated by mice and human cells, suggesting good potential for clinical utilization. We and others have previously demonstrated that PST treatment closely mimics phenotypes fostered by ablation of the plectin gene[18,28,67,68]. Consistently, PST-mediated inhibition of plectin attenuates FAK, MAPK/Erk, and PI3K/Akt pathways in HCC cells with efficacy comparable to CRISPR/Cas-9-engineered functional (ΔIFBD) or full (KO) knockouts. However, despite high PST target selectivity for plectin[67], our data do not rule out pleiotropic effects of PST in the liver and further studies will be required to investigate whether PST mode-of-action in HCC entails molecular mechanisms other than engaging prooncogenic signaling cascades.

Materials and methods

Patient tissue samples

Formalin-fixed paraffin-embedded (FFPE) human liver tissue specimens were prepared at the Department of Surgery of the University Hospital Mannheim. The cohort consisted of 21 patients diagnosed with HCC (for details, see Supplementary file 1). Tissue collection and analysis were performed in accordance with institutional review board guidelines (reference no. 2012-293N-MA), and written informed consent was obtained from all included patients.

Animals

Liver-specific deletion of the plectin (Plec) gene was achieved by crossing *Plectin*$^{flox/flox}$ mice (*Ple*$^{fl/fl}$)[69] with *Alb-Cre* transgenic mice (MGI 2176228; The Jackson Laboratory, Bar Harbor, ME) to generate *Plectin*$^{lox/lox/Alb\text{-}Cre}$(*Ple*$^{\Delta Alb}$) mice[26]. Immunodeficient NOD.Cg-Prkdcscid Il2rgtm1Wjl/SzJ (NSG) mice were purchased from the Czech Centre for Phenogenomics (BIOCEV – Institute of Molecular Genetics Academy of Sciences, Prague, Czechia)

Animals were housed under specific pathogen-free conditions with regular access to chow and drinking water and 12 h light/12 h dark conditions. All animal studies were performed in accordance with European Directive 86/609/EEC and were approved by the Czech Central Commission for Animal Welfare. Age-matched littermate mice were used in all experiments. The details regarding animal treatments can be found in the following sections.

DEN-induced HCC mouse model

2-week-old *Ple*$^{fl/fl}$ and *Ple*$^{\Delta Alb}$ mice received intraperitoneal injection of 25 mg/kg diethylnitrosamine (DEN; Sigma-Aldrich, St. Louis, MO, USA) diluted in PBS. Mice were monitored for tumor formation 30 and 42 weeks after the DEN injection by magnetic resonance imaging (MRI) and tumor volumes were calculated from MRI images (for details see Magnetic resonance imaging section). Mice were sacrificed at 44 weeks post-injection, livers were dissected, and tumors were measured using a caliper.

Lung colonization assay

Huh7 and SNU-475 cell lines stably expressing Red Firefly Luciferase reporter and GFP were prepared by lentiviral transfection of LentiGlo^{TM} pLenti-CMV-RedFluc-IRES-EGFP plasmid (LP-31, Targeting Systems, El Cajon, CA, USA) according to the manufactureŕs protocol. Next, 2×10^6 Huh7 or SNU-475 cells suspended in serum-free Dulbecco's modified Eagle medium (DMEM, Sigma-Aldrich) were injected into the tail vein of 5-week-old NSG mice. The mice were monitored for survival analysis or monitored using bioluminescence imaging for the presence of lung metastasis after 5 weeks. Prior to imaging, mice were anesthetized with isoflurane and injected intraperitoneally with D-luciferin potassium salt (Promega, Madison, WI, USA). Ten to fifteen min after injection, luciferase activity was measured using LagoX (Spectral Instruments Imaging, Tuscon, AZ, USA).

HDTVi-induced HCC mouse model

For hydrodynamic tail vein injections, a mixture of plasmid mix containing 5 µg/ml of px330 expressing Tp53 sgRNA, 5 µg/ml of pT3-EF1a MYC DNA (92046, Addgene, Watertown, MA, USA), and 0.5 µg/ml pCMV HSB2 sleeping beauty transponase was prepared in a sterile 0.9% sodium chloride (NaCl) solution. 7-week-old *Ple*$^{fl/fl}$ and *Ple*$^{\Delta Alb}$ mice were pre-warmed for 15 min using two infrared lamps (IL 11, Beuer GmbH, Ulm, Germany), placed in a restrainer (TV-RED-150_STD, Braintree Scientific INC., Braintree, MA, USA) and injected intravenously via the lateral tail vein

with a total volume corresponding to 10% of body weight over 5–7 s. All animals were monitored daily, and animal experiments were performed in compliance with all relevant ethical regulations outlined in the animal permit. After mice were sacrificed, livers and lungs were visually inspected, excised, and photographed. Tumor samples were taken to obtain protein, and the remaining liver tissue was incubated in 4% PFA for at least 24 h for FFPE tissue preparation.

Statistical analyses

All data mining with the exception of patient analysis, proteomics on mouse tissue samples, and proteomics of SNU-475 cell cultures (see details in corresponding sections), all graphs and statistical tests were performed using GraphPad Prism (GraphPad Software, Inc., La Jolla, CA). In the boxplots, the box margins represent the 25th and 75th percentile with the midline indicates the median. Whiskers reach the last data point. Data comparison of adjacent tumor and non-tumor tissue was performed using a paired *t*-test. Data comparison of individual experimental groups with the control group was performed using a two-tailed *t*-test. Growth curves were analyzed using Two-way ANOVA. Survival curves were analyzed using the Mantel-Cox test. Data distributions were assumed to be normal, but this was not formally tested. Statistical significance was determined at the level of $*P < 0.05$, $**P < 0.01$, < 0.001. The number of independent experiments (N), number of data points (n), and statistical tests used are specified for individual experiments in the figure legends.

For further details regarding the materials used, please refer to the supplementary information.

Acknowledgements

We would like to thank D. Tschaharganeh (DKFZ, Heidelberg) for generously providing the px330 (Tp53 sgRNA) and pT3-EF1a MYC plasmids, and B. Schuster (IMG CAS, Prague) for pX330 Cas9-Venus plasmid; D. Heide and J. Hetzer (DKFZ, Heidelberg) for their outstanding technical assistance; B. Fabry (FAU Erlangen-Nürnberg), K. Volz (DKFZ, Heidelberg), J. Prochazka (Czech Centre for Phenogenomics, Vestec), M. Maninova, M. K. Adamcova, M. Burocziova, M. Capek, and J. Valecka (all IMG CAS, Prague) for their expertise. We acknowledge the Light Microscopy Core Facility, IMG CAS, Prague, Czech Republic, for support with advanced microscopy imaging.

Additional information

Funding

This work was supported by the Grant Agency of the Czech Republic (GA21-21736S and GA24-10672S); the Institutional Research Project of the Czech Academy of Sciences (RVO 68378050); National Institute for Cancer Research (Programme EXCELES, LX22NPO5102) - Funded by the European Union - Next Generation EU; MEYS CR projects (LM2023050, LM2018126, LQ1604 NPU II, LO1419, and LM2015040); and MEYS CR/ERDF projects (OP RDI CZ.1.05/2.1.00/19.0395 and CZ.1.05/1.1.00/02.0109).

Author contributions

Study concept and design: M.G. Acquisition of data: Z.O., G.O.-E., K.K., M.P., L.S., P.B., P.N., P.B., Y.B., A.B., C.G., B.K., A.G., K.S., M.O., O.T., N.J. Analysis and interpretation of data: Z.O., K.K., M.P., L.F., J.K., E.S., D.J., O.T., N.J., D.R., S.M.M., M.G. Drafting of the manuscript: Z.O., M.G. Critical revision of the manuscript for important intellectual content: all authors. Funding: M.G., S.M.M., D.R. Technical and material support: J.K., M.J., M.R., N.R., E.B., A.B., T.O., D.J., M.H., G.W., S.M.M.

Additional files

Supplementary information

References

1 Broders-Bondon F., Nguyen Ho-Bouldoires T. H., Fernandez-Sanchez M. E., Farge E 2018) **Mechanotransduction in tumor progression: The dark side of the force** *J Cell Biol* **217**:1571–1587 https://doi.org/10.1083/jcb.201701039

2 Piersma B., Hayward M. K., Weaver V. M. 2020) **Fibrosis and cancer: A strained relationship.** *Biochim Biophys Acta Rev Cancer* **1873** https://doi.org/10.1016/j.bbcan.2020.188356

3 Cooper J., Giancotti F. G 2019) **Integrin Signaling in Cancer: Mechanotransduction, Stemness, Epithelial Plasticity, and Therapeutic Resistance** *Cancer Cell* **35**:347–367 https://doi.org/10.1016/j.ccell.2019.01.007

4 Hoxhaj G., Manning B. D 2020) **The PI3K-AKT network at the interface of oncogenic signalling and cancer metabolism** *Nat Rev Cancer* **20**:74–88 https://doi.org/10.1038/s41568-019-0216-7

5 Sun Z., Guo S. S., Fassler R. 2016) **Integrin-mediated mechanotransduction.** *J Cell Biol* **215**:445–456 https://doi.org/10.1083/jcb.201609037

6 Dupont S., et al. 2011) **Role of YAP/TAZ in mechanotransduction** *Nature* **474**:179–183 https://doi.org/10.1038/nature10137

7 Esnault C., et al. 2014) **Rho-actin signaling to the MRTF coactivators dominates the immediate transcriptional response to serum in fibroblasts** *Genes Dev* **28**:943–958 https://doi.org/10.1101/gad.239327.114

8 Bustelo X. R 2018) **RHO GTPases in cancer: known facts, open questions, and therapeutic challenges** *Biochem Soc Trans* **46**:741–760 https://doi.org/10.1042/BST20170531

9 Bouameur J. E., Favre B., Borradori L 2014) **Plakins, a versatile family of cytolinkers: roles in skin integrity and in human diseases** *J Invest Dermatol* **134**:885–894 https://doi.org/10.1038/jid.2013.498

10 Prechova M., Korelova K., Gregor M. 2023) **Plectin.** *Curr Biol* **33**:R128–R130 https://doi.org/10.1016/j.cub.2022.12.061

11 Gundesli H., Kori M., Arga K. Y 2023) **The Versatility of Plectin in Cancer: A Pan-Cancer Analysis on Potential Diagnostic and Prognostic Impacts of Plectin Isoforms** *Omics* **27**:281–296 https://doi.org/10.1089/omi.2023.0053

12 Perez S. M., Brinton L. T., Kelly K. A 2021) **Plectin in Cancer: From Biomarker to Therapeutic Target** *Cells* **10** https://doi.org/10.3390/cells10092246

13 Andra K., Nikolic B., Stocher M., Drenckhahn D., Wiche G 1998) **Not just scaffolding: plectin regulates actin dynamics in cultured cells** *Genes Dev* **12**:3442–3451 https://doi.org/10.1101/gad.12.21.3442

14 Nikolic B., Mac Nulty E., Mir B., Wiche G 1996) **Basic amino acid residue cluster within nuclear targeting sequence motif is essential for cytoplasmic plectin-vimentin network**

junctions *J Cell Biol* **134**:1455–1467 https://doi.org/10.1083/jcb.134.6.1455

15 Eisenberg J. L., et al. 2013) **Plectin-containing, centrally localized focal adhesions exert traction forces in primary lung epithelial cells** *J Cell Sci* **126**:3746–3755 https://doi.org/10.1242/jcs.128975

16 Na S., et al. 2009) **Plectin contributes to mechanical properties of living cells** *Am J Physiol Cell Physiol* **296**:C868–877 https://doi.org/10.1152/ajpcell.00604.2008

17 Osmanagic-Myers S., et al. 2015) **Plectin reinforces vascular integrity by mediating crosstalk between the vimentin and the actin networks** *J Cell Sci* **128**:4138–4150 https://doi.org/10.1242/jcs.172056

18 Prechova M., et al. 2022) **Plectin-mediated cytoskeletal crosstalk controls cell tension and cohesion in epithelial sheets** *The Journal of cell biology* **221** https://doi.org/10.1083/jcb.202105146

19 De Pascalis C., et al. 2018) **Intermediate filaments control collective migration by restricting traction forces and sustaining cell-cell contacts** *J Cell Biol* **217**:3031–3044 https://doi.org/10.1083/jcb.201801162

20 Gregor M., et al. 2014) **Mechanosensing through focal adhesion-anchored intermediate filaments** *FASEB J* **28**:715–729 https://doi.org/10.1096/fj.13-231829

21 Wang W., et al. 2020) **Hemidesmosomes modulate force generation via focal adhesions** *J Cell Biol* **219** https://doi.org/10.1083/jcb.201904137

22 Marks P. C., Hewitt B. R., Baird M. A., Wiche G., Petrie R. J 2022) **Plectin linkages are mechanosensitive and required for the nuclear piston mechanism of three-dimensional cell migration** *Mol Biol Cell* **33** https://doi.org/10.1091/mbc.E21-08-0414

23 Vahidnezhad H., et al. 2022) **Mutation update: The spectra of PLEC sequence variants and related plectinopathies** *Human mutation* **43**:1706–1731 https://doi.org/10.1002/humu.24434

24 Boyault S., et al. 2007) **Transcriptome classification of HCC is related to gene alterations and to new therapeutic targets** *Hepatology* **45**:42–52 https://doi.org/10.1002/hep.21467

25 Chiang D. Y., et al. 2008) **Focal gains of VEGFA and molecular classification of hepatocellular carcinoma** *Cancer Res* **68**:6779–6788 https://doi.org/10.1158/0008-5472.CAN-08-0742

26 Jirouskova M., et al. 2018) **Plectin controls biliary tree architecture and stability in cholestasis** *Journal of hepatology* **68**:1006–1017 https://doi.org/10.1016/j.jhep.2017.12.011

27 Xu R., et al. 2022) **Plectin Downregulation Inhibits Migration and Suppresses Epithelial Mesenchymal Transformation of Hepatocellular Carcinoma Cells via ERK1/2 Signaling** *Int J Mol Sci* **24** https://doi.org/10.3390/ijms24010073

28 Meier S. M., et al. 2017) **An Organoruthenium Anticancer Agent Shows Unexpected Target Selectivity For Plectin** *Angewandte Chemie (International ed. in English* **56**:8267–8271 https://doi.org/10.1002/anie.201702242

29 Jiu Y., et al. 2015) **Bidirectional Interplay between Vimentin Intermediate Filaments and Contractile Actin Stress Fibers** *Cell Rep* **11**:1511–1518 https://doi.org/10.1016/j.celrep.2015.05

.008

30 Burgstaller G., Gregor M., Winter L., Wiche G 2010) **Keeping the vimentin network under control: cell-matrix adhesion-associated plectin 1f affects cell shape and polarity of fibroblasts** *Mol Biol Cell* **21**:3362–3375 https://doi.org/10.1091/mbc.E10-02-0094

31 Bodor D. L., Ponisch W., Endres R. G., Paluch E. K 2020) **Of Cell Shapes and Motion: The Physical Basis of Animal Cell Migration** *Dev Cell* **52**:550–562 https://doi.org/10.1016/j.devcel.2020.02.013

32 Yolland L., et al. 2019) **Persistent and polarized global actin flow is essential for directionality during cell migration** *Nat Cell Biol* **21**:1370–1381 https://doi.org/10.1038/s41556-019-0411-5

33 Revia S., et al. 2022) **Histone H3K27 demethylase KDM6A is an epigenetic gatekeeper of mTORC1 signalling in cancer** *Gut* **71**:1613–1628 https://doi.org/10.1136/gutjnl-2021-325405

34 Subramanian A., et al. 2005) **Gene set enrichment analysis: a knowledge-based approach for interpreting genome-wide expression profiles** *Proc Natl Acad Sci U S A* **102**:15545–15550 https://doi.org/10.1073/pnas.0506580102

35 Llovet J. M., et al. 2021) **Hepatocellular carcinoma.** *Nat Rev Dis Primers* **7** https://doi.org/10.1038/s41572-020-00240-3

36 Singal A. G., et al. 2023) **AASLD Practice Guidance on prevention, diagnosis, and treatment of hepatocellular carcinoma** *Hepatology* **78**:1922–1965 https://doi.org/10.1097/HEP.0000000000000466

37 Ladd A. D., Duarte S., Sahin I., Zarrinpar A 2024) **Mechanisms of drug resistance in HCC** *Hepatology* **79**:926–940 https://doi.org/10.1097/HEP.0000000000000237

38 Liu Y. H., et al. 2011) **Cytokeratin 18-mediated disorganization of intermediate filaments is induced by degradation of plectin in human liver cells** *Biochem Biophys Res Commun* **407**:575–580 https://doi.org/10.1016/j.bbrc.2011.03.066

39 Uhlen M., et al. 2017) **A pathology atlas of the human cancer transcriptome** *Science* **357** https://doi.org/10.1126/science.aan2507

40 Flores I. L., et al. 2016) **EEF1D modulates proliferation and epithelial-mesenchymal transition in oral squamous cell carcinoma** *Clin Sci (Lond* **130**:785–799 https://doi.org/10.1042/CS20150646

41 Yang Z., et al. 2019) **Putative biomarkers of malignant transformation of sinonasal inverted papilloma into squamous cell carcinoma** *J Int Med Res* **47**:2371–2380 https://doi.org/10.1177/0300060519838385

42 Paumard-Hernandez B., et al. 2018) **Whole exome sequencing identifies PLEC, EXO5 and DNAH7 as novel susceptibility genes in testicular cancer.** *Int J Cancer* **143**:1954–1962 https://doi.org/10.1002/ijc.31604

43 Yin X., Kong L., Liu P 2021) **Identification of prognosis-related molecular subgroups based on DNA methylation in pancreatic cancer** *Clin Epigenetics* **13** https://doi.org/10.1186/s13148-021-01090-w

44 Strouhalova K., et al. 2020) **Vimentin Intermediate Filaments as Potential Target for Cancer Treatment** *Cancers (Basel* **12** https://doi.org/10.3390/cancers12010184

45 Tolba R., Kraus T., Liedtke C., Schwarz M., Weiskirchen R 2015) **Diethylnitrosamine (DEN)-induced carcinogenic liver injury in mice** *Lab Anim* **49**:59–69 https://doi.org/10.1177/0023677215570086

46 Lee J. S., et al. 2004) **Application of comparative functional genomics to identify best-fit mouse models to study human cancer** *Nat Genet* **36**:1306–1311 https://doi.org/10.1038/ng1481

47 Moon S. H., et al. 2019) **p53 Represses the Mevalonate Pathway to Mediate Tumor Suppression** *Cell* **176**:564–580 https://doi.org/10.1016/j.cell.2018.11.011

48 Buckup M., et al. 2021) **Plectin is a regulator of prostate cancer growth and metastasis** *Oncogene* **40**:663–676 https://doi.org/10.1038/s41388-020-01557-9

49 Pal K., et al. 2017) **Multifaceted peptide assisted one-pot synthesis of gold nanoparticles for plectin-1 targeted gemcitabine delivery in pancreatic cancer** *Nanoscale* **9**:15622–15634 https://doi.org/10.1039/c7nr03172f

50 Perez S. M., Dimastromatteo J., Landen C. N., Kelly K. A 2021) **A Novel Monoclonal Antibody Targeting Cancer-Specific Plectin Has Potent Antitumor Activity in Ovarian Cancer** *Cells* **10** https://doi.org/10.3390/cells10092218

51 Abrahamsberg C., et al. 2005) **Targeted ablation of plectin isoform 1 uncovers role of cytolinker proteins in leukocyte recruitment** *Proc Natl Acad Sci U S A* **102**:18449–18454 https://doi.org/10.1073/pnas.0505380102

52 Zrelski M. M., et al. 2024) **Plectin Deficiency in Fibroblasts Deranges Intermediate Filament and Organelle Morphology, Migration, and Adhesion** *J Invest Dermatol* **144**:547–562 https://doi.org/10.1016/j.jid.2023.08.020

53 Katada K., et al. 2012) **Plectin promotes migration and invasion of cancer cells and is a novel prognostic marker for head and neck squamous cell carcinoma** *J Proteomics* **75**:1803–1815 https://doi.org/10.1016/j.jprot.2011.12.018

54 McInroy L., Maatta A 2011) **Plectin regulates invasiveness of SW480 colon carcinoma cells and is targeted to podosome-like adhesions in an isoform-specific manner** *Exp Cell Res* **317**:2468–2478 https://doi.org/10.1016/j.yexcr.2011.07.013

55 Yoneyama Sutoh, et al. 2014) **Vimentin intermediate filament and plectin provide a scaffold for invadopodia, facilitating cancer cell invasion and extravasation for metastasis** *Eur J Cell Biol* **93**:157–169 https://doi.org/10.1016/j.ejcb.2014.03.002

56 Wenta T., et al. 2022) **Disassembly of alpha6beta4-mediated hemidesmosomal adhesions promotes tumorigenesis in PTEN-negative prostate cancer by targeting plectin to focal adhesions** *Oncogene* **41**:3804–3820 https://doi.org/10.1038/s41388-022-02389-5

57 Bhattacharya R., et al. 2009) **Recruitment of vimentin to the cell surface by beta3 integrin and plectin mediates adhesion strength** *J Cell Sci* **122**:1390–1400 https://doi.org/10.1242/jcs.043042

58 Burch T. C., Watson M. T., Nyalwidhe J. O 2013) **Variable metastatic potentials correlate with differential plectin and vimentin expression in syngeneic androgen independent prostate cancer cells** *PLoS One* **8** https://doi.org/10.1371/journal.pone.0065005

59 Cappuyns S., Corbett V., Yarchoan M., Finn R. S., Llovet J. M 2024) **Critical Appraisal of Guideline Recommendations on Systemic Therapies for Advanced Hepatocellular Carcinoma: A Review** *JAMA oncology* **10**:395–404 https://doi.org/10.1001/jamaoncol.2023.2677

60 Llovet J. M., Montal R., Sia D., Finn R. S 2018) **Molecular therapies and precision medicine for hepatocellular carcinoma** *Nat Rev Clin Oncol* **15**:599–616 https://doi.org/10.1038/s41571-018-0073-4

61 Llovet J. M., et al. 2008) **Sorafenib in advanced hepatocellular carcinoma** *N Engl J Med* **359**:378–390 https://doi.org/10.1056/NEJMoa0708857

62 Yau T., Chan P., Epstein R., Poon R. T 2008) **Evolution of systemic therapy of advanced hepatocellular carcinoma** *World J Gastroenterol* **14**:6437–6441 https://doi.org/10.3748/wjg.14.6437

63 Yau T., et al. 2019) **Nivolumab in advanced hepatocellular carcinoma: Sorafenib-experienced Asian cohort analysis** *J Hepatol* **71**:543–552 https://doi.org/10.1016/j.jhep.2019.05.014

64 Bakewell S. J., et al. 2018) **Suppression of stress induction of the 78-kilodalton glucose regulated protein (GRP78) in cancer by IT-139, an anti-tumor ruthenium small molecule inhibitor** *Oncotarget* **9**:29698–29714 https://doi.org/10.18632/oncotarget.25679

65 Burris H. A., et al. 2016) **Safety and activity of IT-139, a ruthenium-based compound, in patients with advanced solid tumours: a first-in-human, open-label, dose-escalation phase I study with expansion cohort** *ESMO Open* **1** https://doi.org/10.1136/esmoopen-2016-000154

66 Flocke L. S., Trondl R., Jakupec M. A., Keppler B. K 2016) **Molecular mode of action of NKP-1339 - a clinically investigated ruthenium-based drug - involves ER- and ROS-related effects in colon carcinoma cell lines** *Invest New Drugs* **34**:261–268 https://doi.org/10.1007/s10637-016-0337-8

67 Meier-Menches S. M., et al. 2019) **Time-dependent shotgun proteomics revealed distinct effects of an organoruthenium prodrug and its activation product on colon carcinoma cells** *Metallomics* **11**:118–127 https://doi.org/10.1039/c8mt00152a

68 Wernitznig D., et al. 2020) **Plecstatin-1 induces an immunogenic cell death signature in colorectal tumour spheroids** *Metallomics* **12**:2121–2133 https://doi.org/10.1039/d0mt00227e

69 Ackerl R., et al. 2007) **Conditional targeting of plectin in prenatal and adult mouse stratified epithelia causes keratinocyte fragility and lesional epidermal barrier defects** *Journal of cell science* **120**:2435–2443 https://doi.org/10.1242/jcs.004481

Author information

Zuzana Outla
Laboratory of Integrative Biology, Institute of Molecular Genetics of the Czech Academy of Sciences, Prague, Czech Republic
ORCID iD: 0000-0002-8216-4724

Gizem Oyman-Eyrilmez
Laboratory of Integrative Biology, Institute of Molecular Genetics of the Czech Academy of Sciences, Prague, Czech Republic
ORCID iD: 0000-0002-8407-1628

Katerina Korelova
Laboratory of Integrative Biology, Institute of Molecular Genetics of the Czech Academy of Sciences, Prague, Czech Republic
ORCID iD: 0009-0008-6439-5474

Magdalena Prechova
Laboratory of Integrative Biology, Institute of Molecular Genetics of the Czech Academy of Sciences, Prague, Czech Republic
ORCID iD: 0000-0002-4591-854X

Lukas Frick
Institute of Molecular Cancer Research, University of Zurich, Zurich, Switzerland
ORCID iD: 0000-0002-2147-5369

Lenka Sarnova
Laboratory of Integrative Biology, Institute of Molecular Genetics of the Czech Academy of Sciences, Prague, Czech Republic

Piyush Bisht
Laboratory of Integrative Biology, Institute of Molecular Genetics of the Czech Academy of Sciences, Prague, Czech Republic
ORCID iD: 0000-0002-6702-7713

Petra Novotna
Laboratory of Integrative Biology, Institute of Molecular Genetics of the Czech Academy of Sciences, Prague, Czech Republic
ORCID iD: 0000-0003-0018-1975

Jan Kosla
Laboratory of Integrative Biology, Institute of Molecular Genetics of the Czech Academy of Sciences, Prague, Czech Republic, Division of Chronic Inflammation and Cancer, German Cancer Research Center, Heidelberg, Germany
ORCID iD: 0000-0002-1052-4786

Patricia Bortel
Department of Analytical Chemistry, University of Vienna, Vienna, Austria
ORCID iD: 0000-0002-5917-7287

Yasmin Borutzki
Institute of Inorganic Chemistry, University of Vienna, Vienna, Austria
ORCID iD: 0000-0001-9067-4735

Andrea Bileck
Department of Analytical Chemistry, University of Vienna, Vienna, Austria, Joint Metabolome Facility, Medical University of Vienna and University of Vienna, Vienna, Austria
ORCID iD: 0000-0002-7053-8856

Christopher Gerner
Department of Analytical Chemistry, University of Vienna, Vienna, Austria, Joint Metabolome Facility, Medical University of Vienna and University of Vienna, Vienna, Austria
ORCID iD: 0000-0003-4964-0642

Mohammad Rahbari
Division of Chronic Inflammation and Cancer, German Cancer Research Center, Heidelberg, Germany, Department of Surgery, University Hospital Mannheim, Medical Faculty Mannheim, University of Heidelberg, Mannheim, Germany
ORCID iD: 0000-0003-1133-2134

Nuh Rahbari
Department of General and Visceral Surgery, Ulm University Hospital, Ulm, Germany
ORCID iD: 0000-0002-4703-9039

Emrullah Birgin
Department of General and Visceral Surgery, Ulm University Hospital, Ulm, Germany
ORCID iD: 0000-0002-0338-3727

Bibiana Kvasnicova
Department of Natural Sciences, Faculty of Biomedical Engineering, Czech Technical University in Prague, Kladno, Czech Republic

Andrea Galisova
Department of Radiodiagnostic and Interventional Radiology, Institute for Clinical and Experimental Medicine, Prague, Czech Republic
ORCID iD: 0000-0002-0902-2033

Katerina Sulkova
Department of Radiodiagnostic and Interventional Radiology, Institute for Clinical and Experimental Medicine, Prague, Czech Republic
ORCID iD: 0000-0002-0995-149X

Andreas Bauer
Department of Physics, University of Erlangen-Nuremberg, Erlangen, Germany

Njainday Jobe
Department of Cell Biology, Faculty of Science, Charles University, BIOCEV, Vestec, Czech Republic
ORCID iD: 0000-0003-0105-7845

Ondrej Tolde
Department of Cell Biology, Faculty of Science, Charles University, BIOCEV, Vestec, Czech Republic
ORCID iD: 0000-0002-3096-7381

Eva Sticova
Department of Clinical and Transplant Pathology, Institute for Clinical and Experimental Medicine, Prague, Czech Republic, Department of Pathology, Third Faculty of Medicine, Charles University, Prague, Czech Republic
ORCID iD: 0000-0003-2486-6266

Daniel Rosel
Department of Cell Biology, Faculty of Science, Charles University, BIOCEV, Vestec, Czech Republic
ORCID iD: 0000-0001-7221-8672

Tracy O'Connor
Department of Biology, North Park University, Chicago, United States

Martin Otahal
Department of Natural Sciences, Faculty of Biomedical Engineering, Czech Technical University in Prague, Kladno, Czech Republic
ORCID iD: 0000-0002-3282-1941

Daniel Jirak
Department of Radiodiagnostic and Interventional Radiology, Institute for Clinical and Experimental Medicine, Prague, Czech Republic
ORCID iD: 0000-0001-6834-3462

Mathias Heikenwälder
Division of Chronic Inflammation and Cancer, German Cancer Research Center, Heidelberg, Germany
ORCID iD: 0000-0002-3135-2274

Gerhard Wiche
Department of Biochemistry and Cell Biology, Max F. Perutz Laboratories, University of Vienna, Vienna, Austria
ORCID iD: 0000-0001-9550-5463

Samuel M Meier-Menches
Department of Analytical Chemistry, University of Vienna, Vienna, Austria, Institute of Inorganic Chemistry, University of Vienna, Vienna, Austria, Joint Metabolome Facility, Medical University of Vienna and University of Vienna, Vienna, Austria
ORCID iD: 0000-0002-8930-4574

Martin Gregor
Laboratory of Integrative Biology, Institute of Molecular Genetics of the Czech Academy of Sciences, Prague, Czech Republic
ORCID iD: 0000-0001-6841-9527

For correspondence: martin.gregor@img.cas.cz

Editors

Reviewer #1 (Public review):

Summary:

This study investigated the role of PLECTIN, a cytoskeletal crosslinker protein, in liver cancer formation and progression. Using the liver-specific Plectin knockout mouse model, the authors convincingly showed that PLECTIN is critical for hepatocarcinogenesis, as functional inhibition of PLECTIN suppressed tumor formation in several models. They also provided evidence to show that inhibition of PLECTIN inhibited HCC cell invasion and reduced metastatic outgrowth in the lung. Mechanistically, they suggested that PLECTIN inhibition attenuated FAK, MAPK/ERK, and PI3K/AKT signaling.

Strengths:

The authors generated a liver-specific Plectin knockout mouse model. By using DEN and sgP53/MYC models, the authors convincingly demonstrated an oncogenic role of PLECTIN in HCC development. plecstatin-1 (PST), as a plectin inhibitor, showed promising efficacy in inhibiting HCC growth, which provides a basis for potentially treating HCC using PST.

The MIR images for tracking tumor growth in animal models were compelling. The high-quality confocal images and related qualifications convincingly showed the impact of plectin functional inhibition on contractility and adhesions in HCC cells.

Comments on latest version:

My concerns have been largely addressed. The authors did a good job in addressing the questions and clarifying the inconsistent results. I have two comments:

(1) The current data still cannot support the conclusion that plectin inactivation attenuates HCC oncogenic potential through FAK, Erk1/2, and PI3K/Akt axis, unless they can reactivate these signaling to restore the HCC congenic potential in plectin inactivated cells. It might be more appropriate to claim that plectin inactivation suppresses FAK, Erk1/2, and PI3K/Akt oncogenic signaling.

(2) I think it would be beneficial to include the H&E and HNF4α staining from lung tissue of mice inoculated with WT Huh7 cells indicated in the rebuttal letter.

https://doi.org/10.7554/eLife.102205.2.sa3

Reviewer #2 (Public review):

Summary:

Plectin is a cytolinker that associates with cytoskeletal and intercellular junction proteins and is essential for epithelial integrity and cell migration. Previous reports showed that PLEC

regulates tumor growth and metastasis in different cancers. In this manuscript, the authors describe PLEC as a target in initiation and growth of HCC. They show that inhibiting PLEC reduced tumorigenesis in different in vitro and in vivo HCC models, including in a xenograft model, DEN model, oncogene-induced HCC model and a lung metastasis model. A drug PST had similar effects, a purported Plectin inhibitor, suggesting that PLEC inhibition could be a tumor prevention or treatment strategy. Mechanistically, the authors show that inhibiting PLEC results in a disorganized cytoskeleton, deficiency in cell migration, and changes in cancer-relevant signaling pathways. This study demonstrates the importance of understanding mechanobiology of HCC for the development of new treatment strategies.

Strengths:

(1) This study used a variety of in vivo models to explore the role of Plectin in HCC formation and metastasis, which extend beyond the cell line-based studies reported in prior research.
(2) Blocking PLEC disrupts pathways that promote tumors and cell migration, thus preventing tumor progression.
(3) Overall, the anti-cancer phenotype is promising, strengthening the important role of PLEC and related factors in tumor growth and metastasis.

Weaknesses:

(1) There is limited novel mechanistic insights as the effect of inhibiting PLEC on the cytoskeleton, cell migration and related signaling pathways have previously been reported.
(2) The results associated with PST, should be interpretated with caution. Although it is reported as an inhibitor of PLECTIN, and the phenotypes and pathways affected are similar to the knock-out, additional research is needed to support whether it will be safe and specific in treating or preventing HCC.

https://doi.org/10.7554/eLife.102205.2.sa2

Reviewer #3 (Public review):

Summary:

In this manuscript, Outla Z et al described the analysis of Plectin in HCC pathogenesis. Specifically, it was found that elevated Plectin levels in liver tumors, correlated with poor prognosis for HCC patients. Mechanistically, it showed that Plectin-dependent disruption of cytoskeletal networks leads to the attenuation of oncogenic FAK, MAPK/Erk, and PI3K/AKT signals. Finally, the authors showed that Plectin inhibitor plecstatin-1 (PST) is well-tolerated and capable of overcoming therapy resistance in HCC.

Strengths:

The studies of Plectin are not entirely novel (Pubmed: 36613521). Nevertheless, the current manuscript provides a much more detailed mechanistic study and the results have translational implications. Additional strengths include convincing cell biology data, such as Plectin regulates cytoskeletal networks, and HCC migration/invasion.

Comments on latest version:

The authors have addressed my comments.

https://doi.org/10.7554/eLife.102205.2.sa1

Author response:

The following is the authors' response to the original reviews.

Point-by-point responses to the reviewers' comments:

All three reviewers found our analysis of focal adhesion-associated oncogenic pathways (Figs 3 and S3) to be inconsistent (Reviewer 1), not convincing/consistent (Reviewer 2, #2), and too variable and not well supported (Reviewer 3, #2). This was probably the basis for the eLife assessment, which stated: "However, the study is incomplete because the downstream molecular activities of PLECTIN that mediate the cancer phenotypes were not fully evaluated." We agree with the reviewers that the degree of attenuation of the FAK, MAP/Erk, and PI3K/AKT signaling pathways differs depending on the cell line used (Huh7 and SNU-475) and the mode of inactivation (CRISPR/Cas9-generated plectin KO, functional KO (ΔIFBD), and organoruthenium-based inhibitor plecstatin-1). However, we do not share the reviewers' skepticism about the unconvincing nature of the data presented.

Several previous studies have shown that plectin inactivation invariably leads to dysregulation of cell adhesions and associated signaling pathways in various cell systems. The molecular mechanisms driving these changes are not fully understood, but the most convincingly supported scenarios are uncoupling of keratin filaments (hemidesmosomes; (Koster et al., 2004)) and vimentin filaments (focal adhesions; (Burgstaller et al., 2010; Gregor et al., 2014)) from adhesion sites in conjunction with altered actomyosin contractility (Osmanagic-Myers et al., 2015; Prechova et al., 2022; Wang et al., 2020). This results in altered morphometry (Wang et al., 2020), dynamics (Gregor et al., 2014), and adhesion strength (Bonakdar et al., 2015) of adhesions. These changes are accompanied by reduced mechanotransduction capacity and attenuation of downstream signaling such as FAK, Src, Erk1/2, and p38 in dermal fibroblasts (Gregor et al., 2014); decrease in pFAK, pSrc, and pPI3K levels in prostate cancer cells (Wenta et al., 2022); increase in pErk and pSrc in keratinocytes (Osmanagic-Myers et al., 2006); decrease in pERK1/2 in HCC cells (Xu et al., 2022) and head and neck squamous carcinoma cells (Katada et al., 2012).

Consistent with these published findings, we show that upon plectin inactivation, the HCC cell line SNU475 exhibits aberrant cytoskeletal organization (vimentin and actin; Figs 4A-D, S4A-F), altered number, topography and morphometry of focal adhesions (Figs 4A, E-G, S4H,I), and ineffective transmission of traction forces (Fig 4H,I). Similar, although not quantified, phenotypes are present in Huh7 with inactivated plectin (data not shown). It is worth noting, that even robust cytoskeletal (e.g. #ventral stress fibers, Fig 4A,D and vimentin architecture, Fig S4A-C) and focal adhesion (%central FA, Fig 4A,E) phenotypes differ significantly between different modes of plectin inactivation and would certainly do so if compared between cell lines. These phenotypes are heterogeneous but not inconsistent. Interestingly, both SNU-475 and Huh7 plectin-inactivated cells show similar functional consequences such as prominent decrease in migration speed (Fig 5B). This suggests that while specific aspects of cytoarchitecture are differentially affected in different cell lines, the functional consequences of plectin inactivation are shared between HCC cell lines.

It is therefore not surprising that the activation status of downstream effectors, resulting from different degrees of cytoskeletal and focal adhesion reconfiguration, is not identical (or even comparable) between cell lines and treatment conditions. Furthermore, we compare highly epithelial (keratin- and almost no vimentin-expressing) Huh7 cells with highly dedifferentiated (low keratin- and high vimentinexpressing) SNU-475 cells, which differ significantly in their cytoskeleton, adhesions, and signaling networks. Alternative approaches to plectin inactivation are not expected to result in the same degree of dysregulation of specific signaling pathways. Effects of adaptation (CRISPR/Cas9-generated KOs and ΔIFBDs),

engagement of different binding domains (CRISPR/Cas9-generated ΔIFBDs), and pleiotropic modes of action (plecstatin-1) are expected.

In our study, we provide the reader with an unprecedented complex comparison of adhesion-associated signaling between WT and plectin-inactivated HCC cell lines. First, we compared the proteomes of WT, KO and PST-treated WT SNU-475 cells using MS-based shotgun proteomics and phosphoproteomics (Fig 3A-C). Second, we extensively and quantitatively immunoblotted the major molecular denominators of MS-identified dysregulated pathways (such as “FAK signaling”, “ILK signaling”, and “Integrin signaling”) with the following results. Data (shown in Figs 3D and S3C) are expressed as a percentage of untreated WT, with downregulated values are highlighted in red:

Author response table 1.

FAK expression (to GAPDH)	85 (KO) 84 (ΔIFBD) 89 (WT+PST) in Huh7
	82 (KO) 71 (ΔIFBD) 79 (WT+PST) in SNU-475
phospho-Tyr397-FAK (to FAK)	110 (KO) 117 (ΔIFBD) 94 (WT+PST) in Huh7
	104 (KO) 98 (ΔIFBD) 95 (WT+PST) in SNU-475
Akt expression (to GAPDH)	112 (KO) 136 (ΔIFBD) 94 (WT+PST) in Huh7
	91 (KO) 78 (ΔIFBD) 94 (WT+PST) in SNU-475
phospho-Ser473-Akt (to Akt)	84 (KO) 70 (ΔIFBD) 86 (WT+PST) in Huh7 81 (KO) 67 (ΔIFBD) 88 (WT+PST) in SNU-475
Erk1/2 expression (to GAPDH)	119 (KO) 124 (ΔIFBD) 105 (WT+PST) in Huh7
	128 (KO) 170 (ΔIFBD) 86 (WT+PST) in SNU-475
phospho-Thr202/Tyr204-Erk (to Erk)	76 (KO) 78 (ΔIFBD) 90 (WT+PST) in Huh7
	68 (KO) 51 (ΔIFBD) 98 (WT+PST) in SNU-475
ILK expression (to GAPDH)	103 (KO) 102 (ΔIFBD) 87 (WT+PST) in Huh7
	86 (KO) 74 (ΔIFBD) 99 (WT+PST) in SNU-475
PI3K expression (to GAPDH)	108 (KO) 131 (ΔIFBD) 106 (WT+PST) in Huh7
	86 (KO) 84 (ΔIFBD) 82 (WT+PST) in SNU-475
phospho-p85 (Tyr458)/p55(Tyr199)-PI3K (to PI3K)	67 (KO) 54 (ΔIFBD) 72 (WT+PST) in Huh7
	76 (KO) 88 (ΔIFBD) 80 (WT+PST) in SNU-475

In addition, we show dysregulated expression (mostly downregulation) of focal adhesion constituents ITGβ1 and αv, talin, vinculin, and paxilin which nicely complements fewer and larger focal adhesions in plectin-inactivated HCC cells. In light of these results, we believe that our statement that “Although these alterations were not found systematically in both cell lines and conditions (reflecting thus presumably their distinct differentiation grade and plectin inactivation efficacy), collectively these data confirmed plectin-dependent adhesome remodeling together with attenuation of oncogenic FAK, MAPK/Erk, and PI3K/Akt pathways upon plectin inactivation” (see pages 8-9) is fully supported. Furthermore, in support of the results of MS-based (phospho)proteomic and immunoblot analyses we show strong correlation between plectin expression and the signatures of “Integrin pathway” (R^2=0.15, p=

$2x10^{-45}$), "FAK pathway" (R^2=0.11, p= $2x10^{-34}$), "PI3K Akt/mTOR signaling" (R^2=0.06, p= $2x10^{-20}$) or "Erk pathway" (R^2=0.10, p= $6x10^{-30}$) in HCC samples from 1268 patients (Fig S7-2C and S7-3).

In conclusion, we show that plectin is required for proper/physiological adhesion-associated signaling pathways in HCC cells. The HCC adhesome and associated pathways are dysregulated upon plectin inactivation and we show context-dependent varying degrees of attenuation of the FAK, MAPK/Erk, and PI3K/Akt pathways. In our view, presenting context-dependent variability in expression/activation of pathway molecular denominators is a trade-off for our intention to address this aspect of plectin inactivation in the complexity of different cell lines, tissues, and modes of inactivation. We prefer rather this complex approach to presenting "more convincing" black-and-white data assessed in a single cell line (Qi et al., 2022) or upon plectin inactivation by a single approach (compare with otherwise excellent studies such as (Xu et al., 2022) or (Buckup et al., 2021)). In fact, unlike the reviewers, we consider this complexity (and the resulting heterogeneity of the data) to be a strength rather than a weakness of our study.

> ***Reviewer 1:***
>
> *(1) The authors suggest that plectin controls oncogenic FAK, MAPK/Erk, and PI3K/Akt signaling in HCC cells, representing the mechanisms by which plectin promotes HCC formation and progression. However, the effect of plectin inactivation on these signaling was inconsistent in Huh7 and SNU-475 cells (Figure 3D), despite similar cell growth inhibition in both cell lines (Figure 2G). For example, pAKT and pERK were only reduced by plectin inhibition in SNU-475 cells but not in Huh7 cells.*

We agree with the reviewer that plectin inactivation yields varying degrees of attenuation of the FAK, MAPK/Erk, and PI3K/Akt pathways depending on the cell type (Huh7 vs SNU-475 cells) and mode of plectin inactivation (CRISPR/Cas9-generated plectin KO vs functional KO (ΔIFBD) vs organorutheniumbased inhibitor plecstatin-1). This context-dependent heterogeneity in the expression/activation of molecular denominators of signaling pathways reflects different degrees of cytoskeletal (e.g. #ventral stress fibers, Fig 4A,D and vimentin architecture, Fig S4A-C) and focal adhesion (e.g. %central FA, Fig 4A,E) phenotypes under different conditions. We expect, that functional consequences (such as reduced migration and anchorage-independent proliferation) arise from a combination of changes in individual pathways. The sum of often subtle changes will result in comparable effects not only on cell growth, but also on migration or transmission of traction forces. For more detailed comment, please see our response to all Reviewers on the first three pages of this letter.

We believe, that our data show that both pAkt and pErk are attenuated upon plectin inactivation in both Huh7 and SNU-475 cells. The following data (shown in Figs 3D and S3C) are expressed as a percentage of untreated WT, with downregulated values are highlighted in red:

Author response table 2.

phospho-Ser473-Akt (to Akt)	84 (KO) 70 (ΔIFBD) 86 (WT+PST) in Huh7
	81 (KO) 67 (ΔIFBD) 88 (WT+PST) in SNU-475
phospho-Thr202/Tyr204-Erk (to Erk)	76 (KO) 78 (ΔIFBD) 90 (WT+PST) in Huh7
	68 (KO) 51 (ΔIFBD) 98 (WT+PST) in SNU-475

> *(2) In addition, pFAK was not changed by plectin inhibition in both cells, and the ratio of pFAK/FAK was increased in both cells.*

We agree with the reviewer that pFAK/FAK levels are either comparable or slightly higher upon plectin inactivation. However, we believe that our data convincingly show that FAK expression is downregulated in both Huh7 and Snu-475 cells. In our opinion, this results in an overall attenuation of the FAK signaling (see percentage for Normalized pFAKxNormalized FAK), which is expectedly more pronounced in migratory Snu-475 cells. The following data (shown in Figs 3D and S3C) are expressed as a percentage of untreated WT, with downregulated values are highlighted in red:

Author response table 3.

FAK expression (to GAPDH)	85 (KO) 84 (ΔIFBD) 89 (WT+PST) in Huh7
	82 (KO) 71 (ΔIFBD) 79 (WT+PST) in SNU-475
phospho-Tyr397-FAK (to FAK)	110 (KO) 117 (ΔIFBD) 94 (WT+PST) in Huh7
	104 (KO) 98 (ΔIFBD) 95 (WT+PST) in SNU-475
Normalized pFAKxNormalized FAK	94 (KO) 98 (ΔIFBD) 84 (WT+PST) in Huh7
	85 (KO) 70 (ΔIFBD) 75 (WT+PST) in SNU-475

Given these results, we feel that our statement that “inhibition of plectin attenuates FAK signaling” (pages 8-9) is well supported.

> *(3) Thus, it is hard to convince me that plectin promotes HCC formation and progression by regulating these signalings.*

Previous studies have shown that dysregulation of cell adhesions and attenuation of adhesionassociated FAK, MAPK/Erk, and PI3K/Akt signaling has inhibitory effects on HCC formation and progression. We show that plectin is required for the proper/physiological functioning of adhesionassociated signaling pathways in selected HCC cells. The HCC adhesome and associated pathways are dysregulated upon plectin inactivation and we show context-dependent varying degrees of attenuation of the FAK, MAPK/Erk, and PI3K/Akt pathways. We support these conclusions by providing the reader with proteomic and phosphoproteomic comparisons of adhesion-associated signaling between WT and plectin-inactivated HCC cell lines (Figs 3B,C and S3A,B). We further validate our findings by extensive and quantitative immunoblotting analysis (Figs 3D and S3C). In addition, we show a strong correlation between plectin expression and the signatures of “Integrin pathway” (R^2=0.15, p= $2x10^{-45}$), “FAK pathway” (R^2=0.11, p= $2x10^{-34}$), “PI3K Akt/mTOR signaling” (R^2=0.06, p= $2x10^{-20}$) or “Erk pathway” (R^2=0.10, p= $6x10^{-30}$) in HCC samples from 1268 patients (Fig S7E).

Our data and conclusions are fully consistent with previously published studies in HCC cells. For instance, even a mild decrease in FAK levels leads to a significant reduction in colony size (see effects of KD (Gnani et al., 2017) , effects of FAK inhibitor and sorafenib in xenografts (Romito et al., 2021), or effects of inhibitors in soft agars and xenografts (Wang et al., 2016)). Similar effects were observed upon partial Akt inhibition (compare with Akt inhibitors in soft agars (Cuconati et al., 2013; Liu et al., 2020)). Of course, we cannot rule out synergistic plectin-dependent effects mediated via adhesion-independent mechanisms. To identify these mechanisms and to distinguish contribution of various consequences of cytoskeletal

dysregulation to phenotypes described in this manuscript would be experimentally challenging and we feel that these studies go beyond the scope of our current study.

As we feel that the adhesion-independent mechanisms were not sufficiently discussed in the original manuscript, we have removed the original sentence “Given the well-established oncogenic activation of these pathways in human cancer(33), our study identifies a new set of potential therapeutic targets.” (page 15) from the Discussion and added the following text: “However, it is conceivable that dysregulated cytoskeletal crosstalk could affect HCC through multiple mechanisms independent from FA-associated signaling. Indeed, we and others (Jirouskova et al., 2018; Xu et al., 2022) have shown that upon plectin inactivation, liver cells acquire epithelial characteristics that promote increased intercellular cohesion and reduced migration. Further studies will be required to identify and investigate synergistic adhesion-independent effects of plectin inactivation on HCC growth and metastasis.” (page 15). See also our response to Reviewer 2, #4 and Reviewer 3, #3 and #4.

> *(4) The authors claimed that Plectin inactivation inhibits HCC invasion and metastasis using in vitro and in vivo models. However, the results from in vivo models were not as compelling as the in vitro data. The lung colonization assay is not an ideal in vivo model for studying HCC metastasis and invasion, especially when Plectin inhibition suppresses HCC cell growth and survival. Using an orthotopic model that can metastasize into the lung or spleen could be much more convincing for an essential claim.*

We agree with the reviewer that the orthotopic *in vivo* model would be an ideal setting to address HCC metastasis experimentally. There are several published models of HCC extrahepatic metastasis, including an orthotopic model of lung metastasis (Fan et al., 2012; Voisin et al., 2024; You et al., 2016), but to our knowledge, none of these orthotopic models are commonly used in the field. In contrast, the administration of tumor cells via the tail vein of mice is a standard, well-established approach of first choice for modelling lung metastasis in a variety of tumor types (e.g. (Hiratsuka et al., 2011; Jakab et al., 2024; Lu et al., 2020)), including HCC (Jin et al., 2017; Lu et al., 2020; Tao et al., 2015; Zhao et al., 2020).

Furthermore, we do not believe that the use of an orthotopic model would provide a comparable advantage in terms of plectin-mediated effects on metastatic growth compared to tail vein delivery of tumor cells. Importantly, the lung colonization model used in our study allows for the injection of a defined number of HCC cells into the bloodstream, thus eliminating the effect of the primary tumor size on the number of metastasizing cells. To distinguish between effects of plectin inhibition on HCC cell growth/survival and dissemination, we carefully evaluated both the number and volume of lung metastases (Figs 6I and S6C-F). The observed reduction in the number of metastases (Figs 6I and S6D) reflects the initiation/early phase of metastasis formation, which is strongly influenced by the adhesion, migration, and invasion properties of the HCC cells and corresponds well with the phenotypes described after plectin inactivation *in vitro* (Figs 4H,I; 5; 6A-E; S5; and S6A,B). The reduction in the volume of metastases (Figs 6I and S6E) reflects the effects of plectin inhibition on HCC cell growth and metastatic outgrowth and corresponds well with the *in vitro* data shown in Figs 2G,H and S2F,G.

> *(5) Also, in Figure 6H, histology images of lungs from this experiment need to be shown to understand plectin's effect on metastasis better.*

We are grateful to the reviewer for bringing our attention to the lung colonization assay results presented. The description of the experiments in the text of the original manuscript was incorrect. The animals monitored by *in vivo* bioluminescence imaging (shown in Fig 6H) are the same as the mice from which cleared whole lung lobes were analyzed by lattice light sheet fluorescence microscopy (shown in Fig. 6I). The corrected description is now provided in the revised manuscript as follows: “To identify early phase of metastasis formation, we

next monitored the HCC cell retention in the lungs using in vivo bioluminescence imaging (Fig. 6H). This experimental cohort was expanded for WT-injected mice which were administered PST…" (page 11).

Therefore, lungs from all animals shown in Fig 6H,I were CUBIC-cleared and analyzed by lattice light sheet fluorescence microscopy. As requested by Reviewer 2, Recommendation #1, we provide in the revised manuscript (Fig S6F) "whole slide scan results for all the groups" which could help to understand plectin's effect on metastasis better". To address the reviewer's concern, we also post-processed cleared and visualized lungs for hematoxylin staining and immunolabeled them for HNF4α. A representative image is shown as a panel A in Author response image 1. Post-processing of CUBIC-cleared and immunolabeled lung lobes resulted in partial tissue destruction and some samples were lost. In addition, as the entire experimental setup was designed for the early phase of metastasis formation, only small Huh7 foci were formed (compared to the larger metastases that developed within 13 weeks after inoculation shown in the panel B). As the IHC for HNF4α provides significantly lower sensitivity compared to the immunofluorescence images provided in the manuscript, we were only able to identify a few HNF4α-positive foci. Overall, we consider our immunofluorescence images to be qualitatively and quantitatively superior to IHC sections. However, if the reviewer or the editor considers it beneficial, we are prepared to show our current data as a part of the manuscript.

Author response image 1.

(A) HNF4α staining of lung tissue after CUBIC clearing from mice inoculated with WT Huh7 from the timepoint of BLI, when the positive signal in chest area has been detected. This timepoint was then selected for the comparison of initial stages of lung colonization. (B) H&E and HNF4α staining from lung tissue of mice inoculated with WT Huh7 cells from the survival experiment. Scale bars, 50 μm.

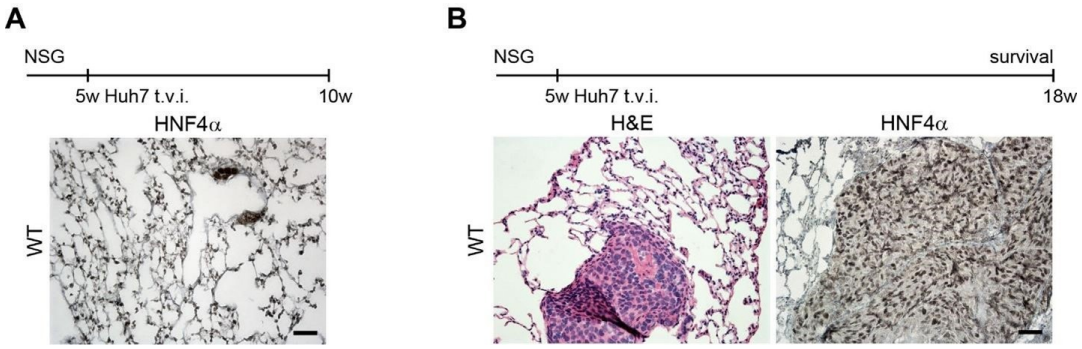

> *(6) Figure 6G, it is unclear how many mice were used for this experiment. Did these mice die due to the tumor burdens in the lungs?*

The number of animals is given in the legend to Fig 6G (page 34; N = 14 (WT), 13 (KO)). Large Huh7 metastases were identified in the lungs of animals that could be analyzed post-mortem by IHC (see panel B in the figure above). No large metastases were found in other organs examined, such as the liver, kidney and brain. It is therefore highly likely that these mice died as a result of the tumor burden in the lungs. A similar conclusion was drawn from the results of the lung colonization model in the previous studies (Jin et al., 2017; Zhao et al., 2020).

> *(7) The whole paper used inhibition strategies to understand the function of plectin. However, the expression of plectin in Huh7 cells is low (Figure 1D). It might be more*

> *appropriate to overexpress plectin in this cell line or others with low plectin expression to examine the effect on HCC cell growth and migration.*

For this study, we selected two model HCC cell lines – Huh7 and SNU-475. Our intention was to investigate the role of plectin in "well-differentiated" (Huh7) and "poorly differentiated" (SNU-475) HCC cells, including thus early and advanced stages of HCC development (as categorized before (Boyault et al., 2007; Yuzugullu et al., 2009a); see also our description and rationale on page 6). As anticipated, less migratory "epithelial-like" Huh7 cells are characterized by relatively high E-cadherin, low vimentin, and low plectin expression levels (Fig 1D). In contrast, migratory "mesenchymal-like" SNU-475 cells are characterized by relatively low E-cadherin, high vimentin, and high plectin expression levels (Fig 1D). Therefore, the majority of analyses were performed in both relatively low plectin-expressing Huh7 and high plectin-expressing SNU-475 cells. It is noteworthy, that inactivation of plectin had similar (although less pronounced) inhibitory effects on growth and migration in both Huh7 and SNU-475 cells.

We agree with the reviewer that "It might be more appropriate to overexpress plectin in this cell line or others with low plectin expression to examine the effect on HCC cell growth and migration". In fact, we have received similar suggestions since we started publishing our studies on plectin. There are two reasons, which preclude the successful overexpression experiments. First, there are about 14 known isoforms of plectin (Prechova et al., 2023). Although, previous studies have analyzed the phenotypic rescue potential of some plectin isoforms using transient transfection (e.g. (Burgstaller et al., 2010; Osmanagic-Myers et al., 2015; Prechova et al., 2022)), the isoform variability precludes rescue/overexpression experiments if the causative isoform is not known. Second, plectin is a giant cytoskeletal crosslinker protein of more than 4,500 amino acids with binding sites for intermediate filaments, F-actin, and microtubules. Overexpression of the approximately 500 kDa-large crosslinker invariably leads to the collapse of cytoskeletal networks in every cell type we have tested so far. See also our response to Reviewer 3, #2.

> ***Reviewer 2:***
>
> *(1) The annotation of mouse numbers is confusing. In Figures 2A B D E F, it should be the same experiment, but the N numbers in A are 6 and 5. In E and F they are 8 and 3. Similarly, in Figure 2H, in the tumor size curve, the N values are 4,4,5,6. In the table, N values are 8,8,10,11 (the authors showed 8,7,8,7 tumors that formed in the picture).*

We are grateful to the reviewer for bringing our attention to the inconsistency the number of animals in DEN-induced hepatocarcinogenesis. Results from two independent cohorts are presented in the manuscript. The first cohort was used for MRI screening (Fig 2A-C) and at the second screening timepoint of 44 weeks, approximately 75% of animals died during anesthesia. Therefore, the second cohort of $Ple^{\Delta Alb}$ and $Ple^{fl/fl}$ mice was used for macroscopic confirmation and histology (Figs 2D-F and S2A). We agree with the reviewer that the original presentation of the data may be misleading; therefore, we have rephrased the sentence describing macroscopic confirmation and histology (Figs 2D-F and S2A) as follows: "Decreased tumor burden in the second cohort of $Ple^{\Delta Alb}$ mice was confirmed macroscopically…" (page 7).

For the experiments shown in Fig 2H, mice were injected in both hind flanks. We have added this information to the figure legend along with the correct number of tumors.

> *(2) In Figure 3D and Figure S3C, the changes in most of the proteins/phosphorylation sites are not convincing/consistent. These data are not essential for the conclusion of the paper and WB is semi-quantitative. Maybe including more plots of the proteins from*

> *proteomic data could strengthen their detailed conclusions about the link between Plectin and the FAK, MAPK/Erk, PI3K/Akt pathways as shown in 3E.*

We agree with the reviewer that plectin inactivation yields varying degrees of attenuation of the FAK, MAPK/Erk, and PI3K/Akt pathways depending on the cell type (Huh7 vs SNU-475 cells) and mode of plectin inactivation (CRISPR/Cas9-generated plectin KO vs functional KO (ΔIFBD) vs organorutheniumbased inhibitor plecstatin-1). This context-dependent heterogeneity in the expression/activation of pathway molecular denominators reflects different degrees of cytoskeletal (e.g. #ventral stress fibers, Fig 4A,D and vimentin architecture, Fig S4A-C) and focal adhesion (e.g. %central FA, Fig 4A,E) phenotypes under different conditions. See also the detailed response to all reviewers (on the first three pages of this letter) and the responses to Reviewer 1, #1 and #2, Reviewer 3, #4.

Our immunoblot analysis is based on NIR fluorescent secondary antibodies which were detected and quantified using an Odyssey imaging system (LI-COR Biosciences). This approach allows a wider linear detection range than chemiluminescence without a signal loss and is considered to provide quantitative immunoblot detection (Mathews et al., 2009; Pillai-Kastoori et al., 2020) (see also manufacturer's website: https://www.licor.com/bio/applications/quantitative-western-blots/).

Following the reviewer's recommendation, we have carefully reviewed our proteomic and phosphoproteomic data. There are no further MS-based data (other than those already presented in the manuscript) to support the association of plectin with the FAK, MAPK/Erk, PI3K/Akt pathways.

> *(3) Figure S7A and B, The pictures do not show any tumor, which is different from Figure 7A and B (and from the quantification in S7A lower right). Is it just because male mice were used in Figure 7 and female mice were used in Figure S7? Is there literature supporting the sex difference for the Myc-sgP53 model?*

As indicated in the Figure legends and in the corresponding text in the Results section (page 12), the Fig 7A,B shows Myc;sgTp53-driven hepatocarcinogenesis in male mice, whereas Fig S7C,D shows results from the female cohort. In general, the HDTVi-induced HCC onset and progression differs considerably between individual experiments, and it is therefore crucial to compare data within an experimental cohort (as we have done for $Ple^{\Delta Alb}$ and $Ple^{fl/fl}$ mice). Nevertheless, we cannot exclude the influence of sexual dimorphism on the results presented. The existence of sexual dimorphism in liver cancer is supported by a substantial body of evidence derived from various studies (e.g. (Bigsby and CaperellGrant, 2011; Bray et al., 2024)). To date, no reports have specifically addressed sexual dimorphism in Myc;sgTp53 HDTVI-induced liver cancer. This is likely due to the fact that the vast majority of studies using this model have only presented data for one sex. However, a study using an HDTVI-administered combination of c-MET and mutated beta-catenin oncogenes to induce HCC in mice observed elevated levels of alpha-fetoprotein (AFP) in males when compared to females (Bernal et al., 2024). The study suggests that estrogen may have a protective effect in female mice, as ovariectomized females had AFP levels comparable to those observed in males. Our data suggest that female hormones may have a similar effect in the Myc;sgTp53 HDTVI-induced liver cancer model.

> *(4) Figure 2F, S2A, $Ple^{\Delta Alb}$ mice more frequently formed larger tumors, as reflected by overall tumor size increase. The interpretation of the authors is "possibly implying reduced migration or increased cohesion of plectin-depleted cells". It is quite arbitrary to make this suggestion in the absence of substantial data or literature to support this theory.*

We agree with the reviewer that our statement "Notably, $Ple^{\Delta Alb}$ mice more frequently formed larger tumors, as reflected by overall tumor size increase (Fig. 2F; Figure 2—figure supplement 1A), possibly implying reduced migration or increased cohesion of plectin-depleted cells(25)." (page 7) is rather speculative. As we did not further address the formation of larger tumors in $Ple^{\Delta Alb}$ mice further in the current study, we wanted to provide the readers with some, even speculative, hypotheses. In support of our hypothesis, we cite our own publication (#26; Jirouskova et al., J Hepatol., 2018), where we show that plectin inactivation in $Ple^{\Delta Alb}$ livers results in upregulation of the epithelial marker E-cadherin. Previous studies have shown that similar increase in E-cadherin expression levels reflects mesenchymalto-epithelial transition (e.g. (Adhikary et al., 2014; Auersperg et al., 1999; Wendt et al., 2011)) and is often associated with reduced cancer cell migration/invasion. This is consistent with our finding that "migrating plectin-disabled SNU-475 cells exhibited more cohesive, epithelial-like features while progressing collectively. By contrast, WT SNU-475 leader cells were more polarized and found to migrate into scratch areas more frequently than their plectin-deficient counterparts (Figure 5—figure supplement 1B). Consistent with this observation, individually seeded SNU-475 cells less frequently assumed a polarized, mesenchymal-like shape upon plectin inactivation in both 2D and 3D environments (Fig. 5C). Moreover, plectin-inactivated SNU-475 cells exhibited a decrease in N-cadherin and vimentin levels when compared to WT counterparts (Figure 5—figure supplement 1C)." (page 10).

In conclusion, we have shown that plectin-deficient hepatocytes express higher levels of E-cadherin and hepatocyte-derived SNU-475 cells express less N-cadherin and vimentin. In addition, we show that SNU475 cells exhibited more cohesive, epithelial-like features in scratch-wound experiments. To address the reviewer's concern and to further support our statement about the increased cohesiveness of plectindeficient HCC cells we have included the citation of the recent study #27 (Xu et al., 2022). Using the MHCC97H and MHCC97L HCC cell lines, this study shows that plectin downregulation "inhibits HCC cell migration and epithelial mesenchymal transformation", which is fully consistent with our hypothesis. To mitigate the impression of an unsubstantiated statement, we also discuss adhesion-independent plectin-mediated mechanisms in the revised Discussion section as follows: "However, it is conceivable that dysregulated cytoskeletal crosstalk could affect HCC through multiple mechanisms independent from FA-associated signaling. Indeed, we and others (Jirouskova et al., 2018; Xu et al., 2022) have shown that upon plectin inactivation, liver cells acquire epithelial characteristics that promote increased intercellular cohesion and reduced migration. Further studies will be required to identify and investigate synergistic adhesion-independent effects of plectin inactivation on HCC growth and metastasis." (page 15).

> *(5) Mutation or KO PLEC has been shown to cause severe diseases in humans and mice, including skin blistering, muscular dystrophy, and progressive familial intrahepatic cholestasis. Please elaborate on the potential side effects of targeting Plectin to treat HCC.*

Indeed, mutation or ablation of plectin has been implicated in many diseases (collectively known as plectinopathies). These multisystem disorders include an autosomal dominant form of epidermolysis bullosa simplex (EBS), limb-girdle muscular dystrophy, aplasia cutis congenita, and an autosomal recessive form of EBS that may be associated with muscular dystrophy, pyloric atresia, and/or congenital myasthenic syndrome. Several mutations have also been associated with cardiomyopathy and malignant arrhythmias. Progressive familial intrahepatic cholestasis has also been reported. In genetic mouse models, loss of plectin leads to skin fragility, extensive intestinal lesions, instability of the biliary epithelium, and progressive muscle wasting (for more details see (Vahidnezhad et al., 2022)).

It is therefore important to evaluate potential side effects, and plectin inactivation therefore presents challenges comparable to other anti-HCC targets. For instance, Sorafenib, the most

widely used chemotherapy in recent decades, targets numerous serine/threonine and tyrosine kinases (RAF1, BRAF, VEGFR 1, 2, 3, PDGFR, KIT, FLT3, FGFR1, and RET) that are critical for proper non-pathological functions (Strumberg et al., 2007; Wilhelm et al., 2006; Wilhelm et al., 2004). The combinatorial therapy of atezolizumab and bevacizumab targets also PD-L1 in conjunction with VEGF, which plays an essential role in bone formation (Gerber et al., 1999), hematopoiesis (Ferrara et al., 1996), or wound healing (Chintalgattu et al., 2003). To allow readers to read a comprehensive account of the pathological consequences of plectin inactivation, we included two additional citations (Prechova et al., 2023; Vahidnezhad et al., 2022) and rephrased Introduction section as follows: "…multiple reports have linked plectin with tumor malignancy(12) and other pathologies (Prechova et al., 2023; Vahidnezhad et al., 2022), mechanistic insights…" (page 4-5).

> ***Reviewer 3:***
>
> *(1) The rationale for using Huh7 cells in the manuscript is not well explained as it has the lowest Plectin expression levels.*

For this study, we selected two model HCC cell lines - Huh7 and SNU-475. Our intention was to address the role of plectin in "well-differentiated" (Huh7) and "poorly differentiated" (SNU-475) HCC cells, thus including early and advanced stages of HCC development (as categorized before (Boyault et al., 2007; Yuzugullu et al., 2009b) see also our description and reasoning on page 6). The Huh7 cell line is also a well-established and widely used model suitable for both *in vitro* and *in vivo* settings (e.g. (Du et al., 2024; Fu et al., 2018; Si et al., 2023; Zheng et al., 2018).

As anticipated, less migratory "epithelial-like" Huh7 cells are characterized by relatively high E-cadherin, low vimentin, and low plectin expression levels (Fig 1D). In contrast, migratory "mesenchymal-like" SNU475 cells are characterized by relatively low E-cadherin, high vimentin, and high plectin expression levels (Fig 1D). Therefore, the majority of analyses were performed in both relatively low plectin-expressing Huh7 and high plectin-expressing SNU-475 cells. It is noteworthy, that inactivation of plectin had similar (although less pronounced) inhibitory effects on the phenotypes in both Huh7 and SNU-475 cells. We believe that these findings highlight the importance of plectin in HCC growth and metastasis, as plectin inactivation has inhibitory effects on both early (low plectin) and advanced (high plectin) stages of HCC.

> *(2) The KO cell experiments should be supplemented with overexpression experiments.*

We agree with the reviewer that it would be helpful to complement our plectin inactivation experiments by overexpressing plectin in the HCC cell lines used in this study. In fact, we have received similar suggestions since we started to publish our studies on plectin. There are two reasons, which preclude the successful overexpression experiments. First, there is about 14 known isoforms of plectin (Prechova et al., 2023). Although previous studies have analyzed the phenotypic rescue potential of some plectin isoforms using transient transfection (e.g. (Burgstaller et al., 2010; Osmanagic-Myers et al., 2015; Prechova et al., 2022)), the isoform variability precludes rescue/overexpression experiments if the causative isoform is not known. Second, plectin is a giant cytoskeletal crosslinker protein of more than 4,500 amino acids with binding sites for intermediate filaments, F-actin, and microtubules. Overexpression of the approximately 500 kDa-large crosslinker invariably leads to the collapse of cytoskeletal networks in every cell type we have tested so far. See also our response to Reviewer 1, #7.

> *(3) There is significant concern that while ablation of Ple led to reduced tumor number, these mice had larger tumors. The data indicate that Plectin may have distinct roles in*

> *HCC initiation versus progression. The data are not well explained and do not fully support that Plectin promotes hepatocarcinogenesis.*

In the DEN-induced HCC model MRI screening revealed fewer tumors and also tumor volume was reduced at 32 and 44 weeks post-induction (Fig 2A-C). Larger tumors formed in $Ple^{\Delta Alb}$ compared to $Ple^{fl/fl}$ livers (Figs 2F and S2A) refer only to a subset of macroscopic tumors visually identified at necropsy. Larger $Ple^{\Delta Alb}$ tumors were not observed in the Myc;sgTp53 HDTVI-induced HCC model (data not shown). In contrast, plectin deficiency reduced the size of xenografts formed in NSG mice (Fig 2H), and agar colonies grown from Huh7 and SNU-475 cells with inactivated plectin were also smaller (Fig S2F). In all *in vivo* and *in vitro* approaches presented in the manuscript, plectin inactivation reduced the number of colonies/xenografts/tumors. As hepatocarcinogenesis is a multistep process including initiation, promotion, and progression (Pitot, 2001), we feel confident in concluding that plectin inactivation inhibits hepatocarcinogenesis and we consider this conclusion to be fully supported by the data presented in the manuscript.

However, we agree with the reviewer that larger macroscopic $Ple^{\Delta Alb}$ tumors in the DEN-induced HCC model are intriguing. As we do not see similar effects (or even trends) in other approaches used in this study, we cannot exclude the contribution of plectin-deficient environment in $Ple^{\Delta Alb}$ livers during longterm (44 weeks) tumor formation and growth. In our previous study (Jirouskova et al., 2018), we showed that plectin deficiency in $Ple^{\Delta Alb}$ livers leads to biliary tree malformations, collapse of bile ducts and ductules, and mild ductular reaction. We could speculate that $Ple^{\Delta Alb}$ livers suffer from continuous bile leakage into the parenchyma, which would exacerbate all models of long-term pathology.

As we did not further address the formation of larger tumors in $Ple^{\Delta Alb}$ mice further in the current study, we offered the reader the hypothesis that large tumors could "…possibly implying reduced migration or increased cohesion of plectin-depleted cells25." In support of our hypothesis, we cite our own publication (#26; Jirouskova et al., J Hepatol., 2018), where we show that plectin inactivation in $Ple^{\Delta Alb}$ livers results in upregulation of the epithelial marker E-cadherin. Previous studies have shown that similar increase in E-cadherin expression levels reflects mesenchymal-to-epithelial transition (e.g. (Adhikary et al., 2014; Auersperg et al., 1999; Wendt et al., 2011)) and is often associated with reduced cancer cell migration/invasion. This is consistent with our finding that "migrating plectin-disabled SNU475 cells exhibited more cohesive, epithelial-like features while progressing collectively. By contrast, WT SNU-475 leader cells were more polarized and found to migrate into scratch areas more frequently than their plectin-deficient counterparts (Figure 5—figure supplement 1B). Consistent with this observation, individually seeded SNU-475 cells less frequently assumed a polarized, mesenchymal-like shape upon plectin inactivation in both 2D and 3D environments (Fig. 5C). Moreover, plectin-inactivated SNU-475 cells exhibited a decrease in N-cadherin and vimentin levels when compared to WT counterparts (Figure 5—figure supplement 1C)." (page 10).

In conclusion, we have shown that plectin-deficient hepatocytes express higher levels of E-cadherin and hepatocyte-derived SNU-475 cells less N-cadherin and vimentin. In addition, we show that SNU-475 cells exhibited more cohesive, epithelial-like features in scratch-wound experiments. To address the reviewer's concern and to further support our claim of increased cohesiveness of plectin-deficient HCC cells we included the citation of the recent study(27). Using the MHCC97H and MHCC97L HCC cell lines, this study shows that plectin downregulation "inhibits HCC cell migration and epithelial mesenchymal transformation" and is therefore fully consistent with our hypothesis. To mitigate the impression of an unsubstantiated statement, we also discuss adhesion-independent plectin-mediated mechanisms in the revised Discussion section as follows: "However, it is conceivable that dysregulated cytoskeletal crosstalk could affect HCC through multiple mechanisms independent from FA-associated signaling. Indeed, we and others (Jirouskova et al., 2018; Xu

et al., 2022) have shown that upon plectin inactivation, liver cells acquire epithelial characteristics that promote increased intercellular cohesion and reduced migration. Further studies will be required to identify and investigate synergistic adhesionindependent effects of plectin inactivation on HCC growth and metastasis." (page 15).

> *(4) Figure 3 showed that Plectin does not regulate p-FAK/FAK expression. Therefore, the statement that Plectin regulates the FAK pathway is not valid. Furthermore, there are too many variables in turns of p-AKT and p-ERK expression, making the conclusion not well supported.*

We agree with the reviewer that pFAK/FAK levels are either comparable or slightly higher upon plectin inactivation. However, we believe that our data convincingly show that FAK expression is downregulated in both Huh7 and Snu-475 cells. In our opinion, this results in an overall attenuation of the FAK signaling (see percentage for Normalized pFAKxNormalized FAK), which is expectedly more pronounced in migratory Snu-475 cells. The following data (shown in Figs 3D and S3C) are expressed as a percentage of untreated WT, with downregulated values highlighted in red:

Author response table 4.

FAK expression (to GAPDH)	85 (KO) 84 (ΔIFBD) 89 (WT+PST) in Huh7
	82 (KO) 71 (ΔIFBD) 79 (WT+PST) in SNU-475
phospho-Tyr397-FAK (to FAK)	110 (KO) 117 (ΔIFBD) 94 (WT+PST) in Huh7
	104 (KO) 98 (ΔIFBD) 95 (WT+PST) in SNU-475
Normalized pFAKxNormalized FAK	94 (KO) 98 (ΔIFBD) 84 (WT+PST) in Huh7
	85 (KO) 70 (ΔIFBD) 75 (WT+PST) in SNU-475

Given these results, we believe that our statement that "inhibition of plectin attenuates FAK signaling" (pages 8-9) is well supported.

We believe, that our data show that both pAkt and pErk are attenuated upon plectin inactivation in both Huh7 and SNU-475 cells. The following data (presented in Figs 3D and S3C) are shown as a percentage of untreated WT, with downregulated values highlighted in red:

Author response table 5.

phospho-Ser473-Akt (to Akt)	84 (KO) 70 (ΔIFBD) 86 (WT+PST) in Huh7
	81 (KO) 67 (ΔIFBD) 88 (WT+PST) in SNU-475
phospho-Thr202/Tyr204-Erk (to Erk)	76 (KO) 78 (ΔIFBD) 90 (WT+PST) in Huh7
	68 (KO) 51 (ΔIFBD) 98 (WT+PST) in SNU-475

We agree with the reviewer that plectin inactivation yields varying degrees of attenuation of the FAK, MAPK/Erk, and PI3K/Akt pathways depending on the cell type (Huh7 vs SNU-475 cells) and mode of plectin inactivation (CRISPR/Cas9-generated plectin KO vs functional KO (ΔIFBD) vs organorutheniumbased inhibitor plecstatin-1). This context-dependent heterogeneity in the expression/activation of pathway molecular denominators reflects

different degrees of cytoskeletal (e.g. #ventral stress fibers, Fig 4A,D and vimentin architecture, Fig S4A-C) and focal adhesion (e.g. %central FA, Fig 4A,E) phenotypes under different conditions. See also the detailed response to all Reviewers (on the first three pages of this letter) and the responses to Reviewer 1, #1 and #2 and Reviewer 2, #4.

> *(5) The studies of plecstatin-1 in HCC should be expanded to a panel of human HCC cells with various Plectin expression levels in turns of cell growth and cell migration. The IC50 values should be determined and correlate with Plectin expression.*

Following the reviewer's suggestion, we have included graphs showing IC50 values for Huh7 (low plectin) and SNU-475 (high plectin) cells as Fig S2E. As expected, the IC50 values are higher for SNU-475 cells. Corresponding parts of the Figure legends have been changed. We refer to new data in the Results section as follows: “If not stated otherwise, we applied PST in the final concentration of 8 μM, which corresponds to the 25% of IC50 for Huh7 cells (Figure 2—figure supplement 1E).” (page 7). We also provide details of the IC50 determination in the revised Supplement Materials and methods section (pages 5-6).

> *(6) One of the major issues is the mechanistic studies focusing on Plectin regulating HCC migration/metastasis, whereas the in vivo mouse studies focus on HCC formation (Figures 3 and 7). These are distinct processes and should not be mixed.*

In our study, we investigated the role of plectin in the development and dissemination of HCC. Using DEN- and Myc;sgTp53 HDTVI-induced HCC models (Figs 2A-F, S2A, 7A-C, and S7A-D), we show the effects of plectin inactivation on HCC formation *in vivo*. These studies are complemented by xenografts (Figs 2H and S2G) and *in vitro* colony formation assay (Figs 2G and S2F). Using an *in vivo* lung colonization assay (Figs 6G-I and S6C-F), we show the effects of plectin inactivation on the metastatic potential of HCC cells. In complementary *in vitro* studies, we show how plectin deficiency affects migration (Figs 5 and S5) and invasion (Figs 6A-E and S6A,B).

Our mechanistic studies show that plectin inactivation leads to dysregulation of cytoskeletal networks, adhesions, and adhesion-associated signaling. We believe that we have provided substantial experimental data suggesting that the proposed mechanisms play a role in plectin-mediated inhibition of both HCC development and dissemination. Of course, we cannot rule out additional, adhesionindependent mechanisms for HCC formation. To clarify this, we have revised the Discussion section as follows: “However, it is conceivable that dysregulated cytoskeletal crosstalk could affect HCC through multiple mechanisms independent from FA-associated signaling. Indeed, we and others (Jirouskova et al., 2018; Xu et al., 2022) have shown that upon plectin inactivation, liver cells acquire epithelial characteristics that promote increased intercellular cohesion and reduced migration. Further studies will be required to identify and investigate synergistic adhesion-independent effects of plectin inactivation on HCC growth and metastasis.” (page 15).

> *(7) Figure 7B showed that Ple KO mice were treated with PST, but the data are not presented in the manuscript. Tumor cell proliferation and apoptosis rates should be analyzed as well.*

We do not show any effects of PST in $Ple^{\Delta Alb}$ mice. As stated in the Fig 7B legend: “Myc;sgTp53 HCC was induced in $Ple^{fl/fl}$, $Ple^{\Delta Alb}$, and PST-treated $Ple^{fl/fl}$ ($Ple^{fl/fl}$+PST) male mice as in (A). Shown are representative images of $Ple^{fl/fl}$, $Ple^{\Delta Alb}$, and $Ple^{fl/fl}$+PST livers from mice with fully developed multifocal HCC sacrificed 6 weeks post-induction.”.

Following the reviewer's recommendation, we include the analysis of proliferation and apoptosis rates as revised Fig S7A,B. Please note, that no differences in apoptosis and

proliferation rates were found between experimental conditions. Due to additional data, the original Fig S7 – 1 has been split into revised Fig S7 – 1 and Fig S7 – 2.

> *(8) The status of FAK, AKT, and ERK pathway activation was not analyzed in mouse liver samples. In Figure 7D, most of the adjusted p-values are not significant.*

We are aware that the majority of FDR corrected p-values shown in the Fig 7D are not significant. In fact, we deliberated with our colleagues from the laboratory of Prof. Samuel Meier-Menches (Department of Analytical Chemistry, University of Vienna), who conducted all the proteomic studies presented in this manuscript, on whether to present such "weak" data. Following a lengthy discussion, a decision was taken to include them despite the anticipation of criticism from the reviewers. The rationale for including these data is that, despite the lack of statistical significance, the findings are consistent with those of MS/immunoblot analyses of HCC cells (Figs 3 and S3) and patient data (Figs 7E, S7-2). The lack of statistical significance observed in the presented data is a consequence of the limited number of animals included in the $Ple^{fl/fl}$, $Ple^{\Delta Alb}$, and PST-treated $Ple^{fl/fl}$ cohorts, which has resulted in a high degree of variability in the MS results. We agree with the reviewer that the inclusion of immunoblot analysis would provide further support for our conclusions. However, we do not have any remaining liver tissue that could be analyzed.

> *(9) There is no evidence to support that PST is capable of overcoming therapy resistance in HCC. For example, no comparison with the current standard care was provided in the preclinical studies.*

We are grateful to the reviewer for bringing our attention to the incorrect statement in the Abstract: “…we show that plectin inhibitor plecstatin-1 (PST) is well-tolerated and capable of overcoming therapy resistance in HCC”. To address the reviewer's concern, we rephrased the Abstract as follows: “…we show that plectin inhibitor plecstatin-1 (PST) is well-tolerated and potently inhibits HCC progression”.

> ***Recommendations for the authors:***
>
> ***Reviewer 2 (Recommendations for the authors):***
>
> *(1) In Figures 6I and S6C, it would be better to show the whole slide scan result for all the groups.*

Following the reviewer's recommendation, we include the whole slide scan result for all the groups as revised Fig S6F.

> *(2) In Figures S7C and D, what do the highlighted/colored dots represent? They are not mentioned in the figure legend or the results.*

Following the reviewer's recommendation, we include the explanation in the revised Figure legends (page 30).

> *(3) In Figure 2H, the experiment schedule showed "6w Huh7 t.v.i.", but should it be subcutaneous injection?*

We are grateful to the reviewer for bringing our attention to the incorrect description of the experiment. The schematics was corrected. The schematic has been corrected. We have also noticed an error in the table summarizing the number of tumors formed (N) and have corrected the values for the WT+PST and KO conditions.

> *(4) Supplemental Materials and Methods, Xenograft tumorigenesis, Error: 2.5×106 Huh7 cells in 250 ml PBS mice were administered subcutaneously in the left and right hind flanks. It probably should be "250ul".*

We are grateful to the reviewer for bringing our attention to the incorrect description of the experiment. The corresponding part of the Materials and Methods section has been corrected (page 2).

> *(5) In Figure legend Supplementary Figure 6 C,D,E : "Representative magnified images from lung lobes with GFP-positive WT, KO, and WT+PST SNU-475 nodules". There is no picture for the WT+PST SNU-475 group.*

We are grateful to the reviewer for bringing our attention to the incorrect description of the experiment. The corresponding part of the Figure legend ("*WT+PST SNU-475*") has been deleted (page 27).

> *(6) In the Figure legend for Figure 6H, "Representative BLI images of WT, KO, and PST-treated WT (WT+PST) SNU-475 cells-bearing mice are shown". Should it be Huh7, not SNU-475?*

We are grateful to the reviewer for bringing our attention to the incorrect description of the experiment. The description of the cell line has been corrected (page 34).

> *(7) The statement that current therapies rely on multikinase inhibitors is no longer correct.*

We are grateful to the reviewer for bringing our attention to the incorrect statement. To address the reviewer's concern, we rephrased the original part of Discussion section: "Current therapies for HCC rely on multikinase inhibitors (such as sorafenib) that provide only moderate survival benefit(60,61) due to primary resistance and the plasticity of signaling networks(62)" as follows: "Current systemic therapies for advanced HCC rely on a combination of multikinase inhibitor (such as sorafenib) or anti-VEGF /VEGF inhibitor (such as bevacizumab) treatment with immunotherapy(59). Multikinase inhibitors provide only moderate survival benefit(60,61) due to primary resistance and the plasticity of signaling networks(62), and only a subset of patients benefits from addition of immunotherapy in HCC treatment(63)" (page 15).

References

Adhikary, A., S. Chakraborty, M. Mazumdar, S. Ghosh, S. Mukherjee, A. Manna, S. Mohanty, K.K. Nakka, S. Joshi, A. De, S. Chattopadhyay, G. Sa, and T. Das. 2014. Inhibition of epithelial to mesenchymal transition by E-cadherin up-regulation via repression of slug transcription and inhibition of Ecadherin degradation: dual role of scaffold/matrix attachment region-binding protein 1 (SMAR1) in breast cancer cells. *The Journal of biological chemistry*. 289:25431-25444.

Auersperg, N., J. Pan, B.D. Grove, T. Peterson, J. Fisher, S. Maines-Bandiera, A. Somasiri, and C.D. Roskelley. 1999. E-cadherin induces mesenchymal-to-epithelial transition in human ovarian surface epithelium. *Proc Natl Acad Sci U S A*. 96:6249-6254.

Bernal, A., M. McLaughlin, A. Tiwari, F. Cigarroa, and L. Sun. 2024. Abstract 772: Investigation of gender disparity in liver tumor formation using a hydrodynamic tail vein injection mouse model. *Cancer Research*. 84:772-772.

Bigsby, R.M., and A. Caperell-Grant. 2011. The role for estrogen receptor-alpha and prolactin receptor in sex-dependent DEN-induced liver tumorigenesis. *Carcinogenesis*. 32:1162-1166.

Bonakdar, N., A. Schilling, M. Sporrer, P. Lennert, A. Mainka, L. Winter, G. Walko, G. Wiche, B. Fabry, and W.H. Goldmann. 2015. Determining the mechanical properties of plectin in mouse myoblasts and keratinocytes. *Exp Cell Res*. 331:331-337.

Boyault, S., D.S. Rickman, A. de Reynies, C. Balabaud, S. Rebouissou, E. Jeannot, A. Herault, J. Saric, J. Belghiti, D. Franco, P. Bioulac-Sage, P. Laurent-Puig, and J. Zucman-Rossi. 2007. Transcriptome classification of HCC is related to gene alterations and to new therapeutic targets. *Hepatology*. 45:42-52.

Bray, F., M. Laversanne, H. Sung, J. Ferlay, R.L. Siegel, I. Soerjomataram, and A. Jemal. 2024. Global cancer statistics 2022: GLOBOCAN estimates of incidence and mortality worldwide for 36 cancers in 185 countries. *CA Cancer J Clin*. 74:229-263.

Buckup, M., M.A. Rice, E.C. Hsu, F. Garcia-Marques, S. Liu, M. Aslan, A. Bermudez, J. Huang, S.J. Pitteri, and T. Stoyanova. 2021. Plectin is a regulator of prostate cancer growth and metastasis. *Oncogene*. 40:663-676.

Burgstaller, G., M. Gregor, L. Winter, and G. Wiche. 2010. Keeping the vimentin network under control: cell-matrix adhesion-associated plectin 1f affects cell shape and polarity of fibroblasts. *Mol Biol Cell*. 21:3362-3375.

Chintalgattu, V., D.M. Nair, and L.C. Katwa. 2003. Cardiac myofibroblasts: a novel source of vascular endothelial growth factor (VEGF) and its receptors Flt-1 and KDR. *J Mol Cell Cardiol*. 35:277-286. Cuconati, A., C. Mills, C. Goddard, X. Zhang, W. Yu, H. Guo, X. Xu, and T.M. Block. 2013. Suppression of AKT anti-apoptotic signaling by a novel drug candidate results in growth arrest and apoptosis of hepatocellular carcinoma cells. *PLoS One*. 8:e54595.

Du, Y.Q., B. Yuan, Y.X. Ye, F.L. Zhou, H. Liu, J.J. Huang, and Y.F. Wei. 2024. Plumbagin Regulates Snail to Inhibit Hepatocellular Carcinoma Epithelial-Mesenchymal Transition in vivo and in vitro. *J Hepatocell Carcinoma*. 11:565-580.

Fan, Z.C., J. Yan, G.D. Liu, X.Y. Tan, X.F. Weng, W.Z. Wu, J. Zhou, and X.B. Wei. 2012. Real-time monitoring of rare circulating hepatocellular carcinoma cells in an orthotopic model by in vivo flow cytometry assesses resection on metastasis. *Cancer Res*. 72:2683-2691.

Ferrara, N., K. Carver-Moore, H. Chen, M. Dowd, L. Lu, K.S. O'Shea, L. Powell-Braxton, K.J. Hillan, and M.W. Moore. 1996. Heterozygous embryonic lethality induced by targeted inactivation of the VEGF gene. *Nature*. 380:439-442.

Fu, Q., Q. Zhang, Y. Lou, J. Yang, G. Nie, Q. Chen, Y. Chen, J. Zhang, J. Wang, T. Wei, H. Qin, X. Dang, X. Bai, and T. Liang. 2018. Primary tumor-derived exosomes facilitate metastasis by regulating adhesion of circulating tumor cells via SMAD3 in liver cancer. *Oncogene*. 37:6105-6118.

Gerber, H.P., T.H. Vu, A.M. Ryan, J. Kowalski, Z. Werb, and N. Ferrara. 1999. VEGF couples hypertrophic cartilage remodeling, ossification and angiogenesis during endochondral bone formation. *Nat Med*. 5:623-628.

Gnani, D., I. Romito, S. Artuso, M. Chierici, C. De Stefanis, N. Panera, A. Crudele, S. Ceccarelli, E. Carcarino, V. D'Oria, M. Porru, E. Giorda, K. Ferrari, L. Miele, E. Villa, C. Balsano, D. Pasini, C. Furlanello, F. Locatelli, V. Nobili, R. Rota, C. Leonetti, and A. Alisi. 2017. Focal adhesion kinase depletion reduces human hepatocellular carcinoma growth by repressing enhancer of zeste homolog 2. *Cell Death Differ*. 24:889-902.

Gregor, M., S. Osmanagic-Myers, G. Burgstaller, M. Wolfram, I. Fischer, G. Walko, G.P. Resch, A. Jorgl, H. Herrmann, and G. Wiche. 2014. Mechanosensing through focal adhesion-anchored intermediate filaments. *FASEB J*. 28:715-729.

Hiratsuka, S., S. Goel, W.S. Kamoun, Y. Maru, D. Fukumura, D.G. Duda, and R.K. Jain. 2011. Endothelial focal adhesion kinase mediates cancer cell homing to discrete regions of the lungs via E-selectin up-regulation. *Proc Natl Acad Sci U S A*. 108:3725-3730.

Jakab, M., K.H. Lee, A. Uvarovskii, S. Ovchinnikova, S.R. Kulkarni, S. Jakab, T. Rostalski, C. Spegg, S. Anders, and H.G. Augustin. 2024. Lung endothelium exploits susceptible tumor cell states to instruct metastatic latency. *Nat Cancer*. 5:716-730.

Jin, H., C. Wang, G. Jin, H. Ruan, D. Gu, L. Wei, H. Wang, N. Wang, E. Arunachalam, Y. Zhang, X. Deng, C. Yang, Y. Xiong, H. Feng, M. Yao, J. Fang, J. Gu, W. Cong, and W. Qin. 2017. Regulator of Calcineurin 1 Gene Isoform 4, Down-regulated in Hepatocellular Carcinoma, Prevents Proliferation, Migration, and Invasive Activity of Cancer Cells and Metastasis of Orthotopic Tumors by Inhibiting Nuclear Translocation of NFAT1. *Gastroenterology*. 153:799-811 e733.

Jirouskova, M., K. Nepomucka, G. Oyman-Eyrilmez, A. Kalendova, H. Havelkova, L. Sarnova, K. Chalupsky, B. Schuster, O. Benada, P. Miksatkova, M. Kuchar, O. Fabian, R. Sedlacek, G. Wiche, and M. Gregor. 2018. Plectin controls biliary tree architecture and stability in cholestasis. *J Hepatol*. 68:1006-1017.

Katada, K., T. Tomonaga, M. Satoh, K. Matsushita, Y. Tonoike, Y. Kodera, T. Hanazawa, F. Nomura, and Y. Okamoto. 2012. Plectin promotes migration and invasion of cancer cells and is a novel prognostic marker for head and neck squamous cell carcinoma. *J Proteomics*. 75:1803-1815.

Koster, J., S. van Wilpe, I. Kuikman, S.H. Litjens, and A. Sonnenberg. 2004. Role of binding of plectin to the integrin beta4 subunit in the assembly of hemidesmosomes. *Mol Biol Cell*. 15:1211-1223.

Liu, H., Q. Chen, D. Lu, X. Pang, S. Yin, K. Wang, R. Wang, S. Yang, Y. Zhang, Y. Qiu, T. Wang, and H. Yu. 2020. HTBPI, an active phenanthroindolizidine alkaloid, inhibits liver tumorigenesis by targeting Akt. *FASEB J*. 34:12255-12268.

Lu, H.H., S.Y. Lin, R.R. Weng, Y.H. Juan, Y.W. Chen, H.H. Hou, Z.C. Hung, G.A. Oswita, Y.J. Huang, S.Y. Guu, K.H. Khoo, J.Y. Shih, C.J. Yu, and H.C. Tsai. 2020. Fucosyltransferase 4 shapes oncogenic glycoproteome to drive metastasis of lung adenocarcinoma. *EBioMedicine*. 57:102846.

Mathews, S.T., E.P. Plaisance, and T. Kim. 2009. Imaging systems for westerns: chemiluminescence vs. infrared detection. *Methods in molecular biology (Clifton, N.J.)*. 536:499-513.

Osmanagic-Myers, S., M. Gregor, G. Walko, G. Burgstaller, S. Reipert, and G. Wiche. 2006. Plectincontrolled keratin cytoarchitecture affects MAP kinases involved in cellular stress response and migration. *J Cell Biol*. 174:557-568.

Osmanagic-Myers, S., S. Rus, M. Wolfram, D. Brunner, W.H. Goldmann, N. Bonakdar, I. Fischer, S. Reipert, A. Zuzuarregui, G. Walko, and G. Wiche. 2015. Plectin reinforces vascular integrity by mediating crosstalk between the vimentin and the actin networks. *J Cell Sci*. 128:4138-4150.

Pillai-Kastoori, L., A.R. Schutz-Geschwender, and J.A. Harford. 2020. A systematic approach to quantitative Western blot analysis. *Analytical biochemistry*. 593:113608.

Pitot, H.C. 2001. Pathways of progression in hepatocarcinogenesis. *Lancet (London, England)*. 358:859860.

Prechova, M., Z. Adamova, A.L. Schweizer, M. Maninova, A. Bauer, D. Kah, S.M. Meier-Menches, G. Wiche, B. Fabry, and M. Gregor. 2022. Plectin-mediated cytoskeletal crosstalk controls cell tension and cohesion in epithelial sheets. *J Cell Biol*. 221.

Prechova, M., K. Korelova, and M. Gregor. 2023. Plectin. *Curr Biol*. 33:R128-R130.

Qi, L., T. Knifley, M. Chen, and K.L. O'Connor. 2022. Integrin alpha6beta4 requires plectin and vimentin for adhesion complex distribution and invasive growth. *J Cell Sci*. 135.

Romito, I., M. Porru, M.R. Braghini, L. Pompili, N. Panera, A. Crudele, D. Gnani, C. De Stefanis, M. Scarsella, S. Pomella, S. Levi Mortera, E. de Billy, A.L. Conti, V. Marzano, L. Putignani, M. Vinciguerra, C. Balsano, A. Pastore, R. Rota, M. Tartaglia, C. Leonetti, and A. Alisi. 2021. Focal adhesion kinase inhibitor TAE226 combined with Sorafenib slows down hepatocellular carcinoma by multiple epigenetic effects. *J Exp Clin Cancer Res*. 40:364.

Si, T., L. Huang, T. Liang, P. Huang, H. Zhang, M. Zhang, and X. Zhou. 2023. Ruangan Lidan decoction inhibits the growth and metastasis of liver cancer by downregulating miR-9-5p and upregulating PDK4. *Cancer Biol Ther*. 24:2246198.

Strumberg, D., J.W. Clark, A. Awada, M.J. Moore, H. Richly, A. Hendlisz, H.W. Hirte, J.P. Eder, H.J. Lenz, and B. Schwartz. 2007. Safety, pharmacokinetics, and preliminary antitumor activity of sorafenib: a review of four phase I trials in patients with advanced refractory solid tumors. *Oncologist*. 12:426-437.

Tao, Q.F., S.X. Yuan, F. Yang, S. Yang, Y. Yang, J.H. Yuan, Z.G. Wang, Q.G. Xu, K.Y. Lin, J. Cai, J. Yu, W.L. Huang, X.L. Teng, C.C. Zhou, F. Wang, S.H. Sun, and W.P. Zhou. 2015. Aldolase B inhibits metastasis through Ten-Eleven Translocation 1 and serves as a prognostic biomarker in hepatocellular carcinoma. *Mol Cancer*. 14:170.

Vahidnezhad, H., L. Youssefian, N. Harvey, A.R. Tavasoli, A.H. Saeidian, S. Sotoudeh, A. Varghaei, H. Mahmoudi, P. Mansouri, N. Mozafari, O. Zargari, S. Zeinali, and J. Uitto. 2022. Mutation update: The spectra of PLEC sequence variants and related plectinopathies. *Human mutation*. 43:17061731.

Voisin, L., M. Lapouge, M.K. Saba-El-Leil, M. Gombos, J. Javary, V.Q. Trinh, and S. Meloche. 2024. Syngeneic mouse model of YES-driven metastatic and proliferative hepatocellular carcinoma. *Dis Model Mech*. 17.

Wang, D.D., Y. Chen, Z.B. Chen, F.J. Yan, X.Y. Dai, M.D. Ying, J. Cao, J. Ma, P.H. Luo, Y.X. Han, Y. Peng, Y.H. Sun, H. Zhang, Q.J. He, B. Yang, and H. Zhu. 2016. CT-707, a Novel FAK Inhibitor, Synergizes with Cabozantinib to Suppress Hepatocellular Carcinoma by Blocking Cabozantinib-Induced FAK Activation. *Mol Cancer Ther*. 15:2916-2925.

Wang, W., A. Zuidema, L. Te Molder, L. Nahidiazar, L. Hoekman, T. Schmidt, S. Coppola, and A. Sonnenberg. 2020. Hemidesmosomes modulate force generation via focal adhesions. *J Cell Biol*. 219.

Wendt, M.K., M.A. Taylor, B.J. Schiemann, and W.P. Schiemann. 2011. Down-regulation of epithelial cadherin is required to initiate metastatic outgrowth of breast cancer. *Mol Biol Cell*. 22:24232435.

Wenta, T., A. Schmidt, Q. Zhang, R. Devarajan, P. Singh, X. Yang, A. Ahtikoski, M. Vaarala, G.H. Wei, and A. Manninen. 2022. Disassembly of alpha6beta4-mediated hemidesmosomal adhesions promotes tumorigenesis in PTEN-negative prostate cancer by targeting plectin to focal adhesions. *Oncogene*. 41:3804-3820.

Wilhelm, S., C. Carter, M. Lynch, T. Lowinger, J. Dumas, R.A. Smith, B. Schwartz, R. Simantov, and S. Kelley. 2006. Discovery and development of sorafenib: a multikinase inhibitor for treating cancer. *Nat Rev Drug Discov*. 5:835-844.

Wilhelm, S.M., C. Carter, L. Tang, D. Wilkie, A. McNabola, H. Rong, C. Chen, X. Zhang, P. Vincent, M. McHugh, Y. Cao, J. Shujath, S. Gawlak, D. Eveleigh, B. Rowley, L. Liu, L. Adnane, M. Lynch, D. Auclair, I. Taylor, R. Gedrich, A. Voznesensky, B. Riedl, L.E. Post, G. Bollag, and P.A. Trail. 2004. BAY 43-9006 exhibits broad spectrum oral antitumor activity and targets the RAF/MEK/ERK pathway and receptor tyrosine kinases involved in tumor progression and angiogenesis. *Cancer Res*. 64:7099-7109.

Xu, R., S. He, D. Ma, R. Liang, Q. Luo, and G. Song. 2022. Plectin Downregulation Inhibits Migration and Suppresses Epithelial Mesenchymal Transformation of Hepatocellular Carcinoma Cells via ERK1/2 Signaling. *Int J Mol Sci*. 24.

You, A., M. Cao, Z. Guo, B. Zuo, J. Gao, H. Zhou, H. Li, Y. Cui, F. Fang, W. Zhang, T. Song, Q. Li, X. Zhu, H. Yin, H. Sun, and T. Zhang. 2016. Metformin sensitizes sorafenib to inhibit postoperative recurrence and metastasis of hepatocellular carcinoma in orthotopic mouse models. *J Hematol Oncol*. 9:20.

Yuzugullu, H., K. Benhaj, N. Ozturk, S. Senturk, E. Celik, A. Toylu, N. Tasdemir, M. Yilmaz, E. Erdal, K.C. Akcali, N. Atabey, and M. Ozturk. 2009a. Canonical Wnt signaling is antagonized by noncanonical Wnt5a in hepatocellular carcinoma cells. *Molecular Cancer*. 8:90.

Yuzugullu, H., K. Benhaj, N. Ozturk, S. Senturk, E. Celik, A. Toylu, N. Tasdemir, M. Yilmaz, E. Erdal, K.C. Akcali, N. Atabey, and M. Ozturk. 2009b. Canonical Wnt signaling is antagonized by noncanonical Wnt5a in hepatocellular carcinoma cells. *Mol Cancer*. 8:90.

Zhao, J., Y. Hou, C. Yin, J. Hu, T. Gao, X. Huang, X. Zhang, J. Xing, J. An, S. Wan, and J. Li. 2020. Upregulation of histamine receptor H1 promotes tumor progression and contributes to poor prognosis in hepatocellular carcinoma. *Oncogene*. 39:1724-1738.

Zheng, H., Y. Yang, C. Ye, P.P. Li, Z.G. Wang, H. Xing, H. Ren, and W.P. Zhou. 2018. Lamp2 inhibits epithelial-mesenchymal transition by suppressing Snail expression in HCC. *Oncotarget*. 9:3024030252.

https://doi.org/10.7554/eLife.102205.2.sa0